The sulfur-related metabolic status of *Aspergillus fumigatus* during infection reveals cytosolic serine hydroxymethyltransferase as a promising antifungal target.

In vivo transcriptomics to identify new antifungal targets and validation of SHMT

Reem Alharthi[1], Monica Sueiro-Olivares[1], Isabelle Storer[1], Hajer Bin Shuraym [1¥], Jennifer Scott[1], Reem Al-Shidhani[2], Rachael Fortune-Grant[1], Elaine Bignell[3], Lydia Tabernero[2], Michael Bromley[1], Can Zhao[4], and Jorge Amich[1,5]*

1. Manchester Fungal Infection Group (MFIG), Division of Evolution, Infection, and Genomics, Faculty of Biology, Medicine and Health, University of Manchester, Manchester, M13 9PT UK.
2. Lydia Becker Institute for Immunology and Inflammation. School of Biological Sciences, Faculty of Biology Medicine and Health, Manchester Academic Health Science Centre, University of Manchester, Manchester M13 9PT, UK
3. MRC Centre for Medical Mycology, University of Exeter, Exeter, EX4 4QD, UK.
4. Department of Life Sciences, Manchester Metropolitan University, Manchester, M1 5GD, United Kingdom.
5. Mycology Reference Laboratory (Laboratorio de Referencia e Investigación en Micología LRIM), National Centre for Microbiology, Instituto de Salud Carlos III (ISCIII), Majadahonda, 28220 Madrid, Spain.

¥. Current affiliation: Department of Clinical Laboratory Sciences, College of Applied Medical Sciences, King Saud Bin Abdulaziz University for Health Sciences, P.O. Box 3660, Riyadh 11481, Saudi Arabia. King Abdullah International Medical Research Center, Riyadh, Saudi Arabia.

*Correspondence to Jorge Amich: jamich@isciii.es

ABSTRACT

Sulfur metabolism is an essential aspect of fungal physiology and is known to be crucial for pathogenicity. Fungal sulfur metabolism comprises anabolic and catabolic routes that are not well-conserved in mammals, and therefore can be considered a promising source of prospective novel antifungal targets. To gain insight into the status of the *Aspergillus fumigatus* sulfur-related metabolism during infection we used a NanoString custom nCounter TagSet and compared the expression of 68 key metabolic genes in different murine models of invasive pulmonary aspergillosis, at three different time-points, and a variety of *in vitro* conditions. We identified a set of 15 genes that are consistently expressed at higher levels *in vivo* than *in vitro*, suggesting that they may be particularly relevant for intrapulmonary growth and therefore constitute promising drug targets. Indeed, the role of five of the fifteen genes had previously been empirically validated, supporting the likelihood that the remaining candidates are relevant. In addition, the analysis of the dynamics of gene expression at the early (16h), mid (24h-1) and late (72h) time-points uncovered potential disease initiation and progression factors. We further characterised one of the identified genes, encoding the cytosolic serine hydroxymethyltransferase ShmB, and demonstrated that it is an essential gene of *A. fumigatus* and that it is also required for virulence in a murine model of established pulmonary infection. We further show that the structure of the ligand binding pocket of the fungal enzyme differs significantly from its human counterpart, suggesting that specific inhibitors can be designed. Therefore, *in vivo* transcriptomics is a powerful tool to identify genes crucial for fungal pathogenicity that might encode promising antifungal target candidates.

AUTHOR SUMMARY

Aspergillus fumigatus is an opportunistic human fungal pathogen that causes devastating chronic and invasive infections in immunocompromised patients. Our arsenal of antifungal drugs to fight this and other fungal pathogens is very limited, partly because of the high similarity between eukaryotic fungal and human cells makes the identification of suitable drug targets a challenging task. Furthermore, targets identified *in vitro* are often not effective *in vivo*, as their action is not relevant for fungal virulence. To address this challenge, we compared the expression profiles of a set of genes involved in sulfur metabolism, a promising source of potential drug targets, in numerous *in vitro* and *in vivo* conditions to identify favourable antifungal candidates. Subsequently, we validated one of the highlighted genes, demonstrating that it is essential for *A. fumigatus* viability and virulence, and that it can likely be targeted by specific inhibitors. Hence, we show the potential of using *in vivo* transcriptomics to identify targets that contribute to virulence, propose various candidates for future studies and present a novel target validated for further antifungal drug development.

64 **INTRODUCTION**

65 *Aspergillus fumigatus* is a ubiquitous mould that normally lives in the soil feeding on decaying organic
66 matter [1]. During its natural life-cycle *A. fumigatus* produces thousands of spores, also known as
67 conidia, that are disseminated in the air. Because of their high abundance and prevalence, it has been
68 estimated that every human breathes in several hundred of these conidia on a daily basis [2] and, due
69 to their small size (2-3 µm), they have the potential to penetrate deep into the respiratory tract and
70 even reach the lung alveoli [3]. In immunocompetent individuals, this has no consequence as epithelial
71 mucocilliarity and a proper immune response eliminate the spores very efficiently [4]. However,
72 patients with an imbalanced immune response are susceptible to *A. fumigatus*, which can cause a
73 wide range of diseases collectively termed aspergilloses [5]. Chronic and invasive aspergilloses are life-
74 threatening infections with high mortality rates, even in patients under antifungal treatment [6, 7].
75 First line therapy against aspergilloses is based on the use of azoles, the only class of antifungals that
76 can be orally administered. Worryingly, the number of clinical *A. fumigatus* isolates that are resistant
77 to triazole antifungals is increasing worldwide, which correlates with higher mortality rates [6, 8, 9].
78 Consequently, new agents to fight this fungal pathogen are urgently required.

79 Metabolism is central to the virulence of fungal pathogens, and therefore its targeting is considered a
80 promising strategy for the development of novel antifungals [10, 11]. Fungal sulfur metabolism is
81 particularly interesting as it comprises routes and enzymes that are often not conserved in humans,
82 and thus it is considered a propitious source of novel antifungal targets [12]. Indeed, we have
83 previously shown that a proper regulation of sulfur metabolism is crucial for *A. fumigatus* infective
84 capacity [13], demonstrated that biosynthesis of the S-containing amino acids is required for virulence
85 [14], and comprehensively characterised an enzyme in the trans-sulfuration pathway, methionine
86 synthase, as a promising antifungal target [15]. Others have also shown that sulfur is involved in the
87 biosynthesis of essential fungal metabolites [16] and proposed sulfur assimilation and the trans-
88 sulfuration pathway as sources of antifungal targets [17, 18]. Here, we aimed to expand on that
89 knowledge by using *in vivo* transcriptomics to better characterise the fungal sulfur metabolic status
90 during infection of the murine lung, and to use the expression profile of genes to identify those that
91 may be relevant for infection, proposing them as promising candidates for further investigations.
92 However, detection and analysis of the fungal transcriptome during infection is a persistent challenge,
93 as fungal RNA usually represents only between 0.05 and 0.5% of the total RNA isolated from infected
94 organs [19]. To overcome this obstacle, we have used NanoString nCounter, a novel probe-based
95 technology with excellent reproducibility, sensitivity, and specificity when compared to other
96 transcriptomic methods such as microarray hybridisation or RT-qPCR [20, 21]. Its high sensitivity, being
97 capable of detecting mRNA concentrations in the femtomolar range [22], makes this technology ideal

98 for detecting and quantifying fungal RNA during infection. Furthermore, its incomparable specificity is
99 fundamental to prevent any crosstalk with the abundant host RNA. Using this technology, we have
100 assessed the transcription profile of a selection of metabolic genes during infection of the murine lung
101 in two models of immunosuppression and at three time-points post infection, and compared them
102 with the expression profiles under a variety of *in vitro* conditions. By these means we have uncovered
103 interesting aspects of the *in vivo* sulfur metabolic status and identified genes that can be proposed as
104 relevant for growth in the tissues. We have further characterised a promising candidate, the cytosolic
105 serine hydroxymethyltransferase (*shmB*) encoding gene, demonstrating that it is essential for *A.*
106 *fumigatus* viability as well as for virulence and that it is promising to aim for the development of
107 fungal-specific inhibitors against this target, which can serve to address the emerging global threat of
108 antifungal resistance [23, 24].

109

110 **RESULTS**

111 *Linear amplification of Aspergillus fumigatus mRNAs allows gene expression profiling of low input in*
112 *vivo samples.*

113 To determine the transcriptional status of genes related to sulfur metabolism during fungal infection
114 of the murine lung, we developed a custom NanoString nCounter Elements TagSet comprising 68
115 metabolic genes (51 directly related to S-metabolism and 17 metabolic genes of interest indirectly
116 related with S-metabolism) and 4 housekeeping controls (Table S1). We isolated RNA from *A.*
117 *fumigatus* propagated under a variety of *in vitro* conditions (Table S2) and from the lungs of infected
118 mice immunosuppressed with two different regimens, the leukopenic and the corticosteroid model
119 (Table S2 and see material and methods). We isolated the lungs of infected mice at three different
120 time-points to investigate gene expression at an early (16h), medium (24h) and late (72h) time point
121 of infection (3 mice per time-point). We further assayed a chronic model of pulmonary aspergillosis
122 [25] to determine if this model provides a significantly different S-environment (Table S2). A
123 preliminary experiment revealed that fungal RNA could not be reliable detected at 16h and 24h post-
124 infection, which is expected as the fungal burden at those early times is very low. To circumvent this
125 problem, we applied the Nanostring Single Cell Gene Expression protocol (see Material and Methods)
126 to perform linear amplification using Multiplexed Target Enrichment (MTE) primers. To verify that the
127 MTE enrichment does not affect the relative abundance of transcripts, we compared the fold changes
128 between diluted-amplified and non-amplified (undiluted) *in vitro* (-S limiting conditions) and *in vivo*
129 samples (lungs extracted from two leukopenic mice 72h after infection) (Fig 1A). This direct
130 comparison demonstrated that the correlation of the fold changes detected with non-amplified and

131 amplified samples was very high (R^2=0.95 for mouse 1 and R^2=0.84 for mouse 2). Therefore, MTE
132 enrichment of low input fungal RNA samples does not affect the relative abundance of transcripts and
133 can be used to investigate gene expression in the mammalian lung at early time-points after infection.

134

135 *The fungal S-related metabolic status in vivo is different from that of in vitro conditions, revealing*
136 *genes potentially relevant for infection*

137 To analyse the S-related fungal metabolic status *in vivo* and *in vitro*, we hybridized and read our
138 custom NanoString codeset with isolated RNAs or amplified cDNAs (Table S2). The obtained raw data
139 was subjected to quality control, which revealed that the samples obtained from two leukopenic mice
140 72h had not run properly: they were borderline for the recommended threshold of overall number of
141 counts (10,000) and did not reach the minimum values for the positive counts reads (Fig. S1A and S1B).
142 Consequently, these samples were excluded from all analyses. In addition, inspection of the
143 normalized data (see Material and Methods for details) revealed that five genes (AFUA_3G06492,
144 AFUA_1G06940, AFUA_5G08600, AFUA_4G03950 and AFUA_6G00760) had a very low number of
145 counts (<20) in all samples. This could be due to the genes not being expressed at all or at very low
146 levels in the tested conditions, or to failure of the NanoString designed probes to detect these mRNAs.
147 Accordingly, these genes were also excluded from all downstream analyses.

148 We first performed an unsupervised hierarchical clustering of all samples analysed (Fig. 1B). By this
149 stratification, the *in vivo* samples clearly clustered separately from the *in vitro* samples, indicating that
150 the fungal S-related metabolic status during infection is significantly different from that during growth
151 in diverse experimental conditions This suggests that the lung provides a unique environment in terms
152 of sulfur metabolism that is clearly distinct from defined culture media, despite our efforts to provide
153 potentially relevant sulfur sources. Noteworthy, this also included the two S-depleted samples, which
154 indicates that the mammalian lung is not sulfur limiting. Based on this, we hypothesised that genes
155 which are consistently more highly expressed *in vivo*, compared to in the great variety of tested *in*
156 *vitro* conditions, may be particularly relevant for the fungal capacity to grow in the lung tissues, and
157 therefore for fungal virulence. We detected a cluster of 15 genes which were always expressed more
158 *in vivo* than *in vitro* (Fig. 1B, red box, Table 1). Interestingly, we and others have already demonstrated
159 the importance of at least five of those genes for *A. fumigatus* virulence, and a further six genes had
160 already been proposed to be potentially relevant (Table 1 and see discussion), supporting the rationale
161 that the uncharacterized genes might be valid candidates for further analyses.

162

GENE ID	DESCRIPTION	VIRULENCE
AFUA_1G11980	Glutamine amidotransferase (HisfF/H)	Suspected [26]
AFUA_8G02500	Glutathione S-transferase	Suspected [27]
AFUA_3G06530	ATP sulfurylase (sC)	Unknown
AFUA_5G02180	Cysteine synthase (CysB)	Proven [14]
AFUA_3G09320	Serine hydroxymethyltransferase (SmhB)	This work
AFUA_1G17170	Taurine dioxygenase	Unknown
AFUA_3G13900	Glutamate-cysteine ligase (Gcs1)	Suspected [27]
AFUA_5G03920	bZIP transcription factor (HapX)	Proven [28]
AFUA_2G07680	L-ornithine N5-oxygenase (SidA)	Proven [29]
AFUA_4G12470	bZIP transcription factor (CpcA)	Proven [30]
AFUA_6G08790	C6 transcription factor (PrnA)	Unknown
AFUA_5G06060	SCF-complex subunit (SkpA)	Suspected [31, 32]
AFUA_8G04340	cystathionine gamma-lyase (MecB)	Proven [33]
AFUA_7G06810	L-amino acid oxidase (LaoA)	Suspected [34]
AFUA_2G07620	Cystathionine beta-synthase (mecA)	Suspected [33]

Table 1. Genes that consistently showed higher expression *in vivo* compared to any of the tested *in vitro* conditions.

Fungal sulfur related in vivo metabolism is influenced by the model of immunosuppression and the course of infection.

To investigate if the fungal S-related metabolic status is influenced by the model of immunosuppression, we performed hierarchical clustering of all the *in vivo* samples (Fig. 2A). This clustering showed that the fungal S-related status is quite variable *in vivo* (notice that the dynamic range of expression are much smaller than when comparing *in vitro* and *in vivo* samples in Fig. 1B), and is partially dependent on the model of immunosuppression, as 5 out of the 8 leukopenic mice aggregated in a separated cluster. Interestingly, the chronic model clustered in this separated branch, suggesting that the fungal S-related metabolic status in this type of infection is more similar to the status in the leukopenic model than in the steroid-induced one. Nevertheless, some samples from leukopenic mice interleaved with the samples from steroid-treated mice, demonstrating that the model of immunosuppression is not the only factor that determines the fungal metabolic status.

To investigate to what extent the fungal S-related metabolic status is influenced by the course of infection, we performed hierarchical clustering of the samples from leukopenic and steroid-treated mice separately (Fig 2B). In both models of suppression there was a partial aggregation of samples according to the time point post infection, suggesting that the course of infection is mirrored by the S-related metabolic status of the fungal pathogen.

184 In conclusion, the model of immunosuppression as well as the time of duration of infection appear to
185 influence the status of the fungal S-related metabolism. However, these variables alone or combined
186 cannot explain the variances among samples, indicating that other factors must be involved. For
187 instance, it is to be expected that the exact anatomic location of the foci of fungal growth would
188 account for different microenvironments that in turn affect the fungal S-related metabolism.

189

190 *Temporal dynamics of gene expression in vivo versus in vitro reveals the existence of potential disease*
191 *initiation and progression factors*

192 Since we found that the S-related metabolic status correlates with the time period post infection, we
193 reasoned that some genes may be expressed at different levels as the fungal infection progresses. To
194 investigate this hypothesis, we first examined the fold change of the (geometric) mean expression of
195 all genes in each time-point with respect to the corresponding 16h condition (Fig. 3A). This analysis
196 revealed that indeed many genes change the level of expression during the course of infection:
197 transcription of several genes seemed to consistently increase, a few decreased expression as
198 infection progressed, and some appeared to increase or decrease expression at mid-infection (24h)
199 before returning to initial levels in late infection (72h). To explore whether any of these genes that
200 show temporal dynamic expression could be particularly important for *in vivo* growth, we analysed
201 the fold change of all genes in each *in vitro* condition versus each of the leukopenic (Fig. S2A) or
202 steroid-treated (Fig. S2B) samples grouped by the time after infection. As expected, we identified
203 some genes which showed a temporal variance *in vivo* compared with *in vitro*. In detail, in leukopenic
204 mice we observed that genes *metAT* (AFUA_2G13630), *cdoB* (AFUA_5G14410), *cysAT*
205 (AFUA_1G09470), *isa1* (AFUA_4G10690) and *hisB* (AFUA_6G04700) had higher transcript levels *in vivo*
206 at early (16h) than at mid (24h) or late (72h) time points after infection (Fig. 3B and Fig. S2A orange
207 boxes), suggesting that these genes may be particularly important for the initiation of infection, but
208 possibly not as relevant for progression and maintenance of infection. In contrast, *cdoA*
209 (AFUA_1G05570) had higher *in vivo* transcription during advanced infection (Fig. 3C and Fig. S2A
210 purple box), suggesting that this gene may be relevant for growth in progressively invaded tissue. The
211 genes, *sD* (AFUA_1G10820), *metR* (AFUA_4G06530) and *hapX* (AFUA_5G03920) displayed higher
212 expression at early (16h) and late (72h) time after infection (Fig. 3D and Fig. S2A black box), suggesting
213 that they may be particularly important to initiate infection and during established infection, but that
214 they are not crucial for infection to progress.

215 Similarly, in steroid treated mice, we observed that genes *metAT* (AFUA_2G13630), *cysAT*
216 (AFUA_1G09470), *isa1* (AFUA_4G10690) and *ssuA* (AFUA_7G01790) had higher expression at mid-

217 (24h) and late (72h) times after infection (Fig. 3E and Fig. S2B purple box), indicating that they may be
218 more relevant for progression and maintenance of infection than for its initiation. Finally, genes *sFα*
219 (AFUA_6G08920), *sB* (AFUA_1G05020), *sA* (AFUA_3G06540), *mupA* (AFUA_4G09040), *mupB*
220 (AFUA_7G00730), *sfnB* (AFUA_8G01010), two taurine dioxygenase encoding genes (AFUA_3G0796
221 and AFUA_3G01010) and one arylsulfatase encoding gene (AFUA_8G02520) had higher expression *in*
222 *vivo* at mid-infection time (24h) (Fig. 3G and Fig. S2B orange boxes), suggesting that these genes may
223 play a role in this model for the progression of infection.

224 We therefore propose that the temporal dynamics of *in vivo* transcript levels may be useful to identify
225 and differentiate fungal factors of disease initiation and progression, defined as products that are
226 essential for the initiation of infection or that facilitate persistence and continued disease progression
227 [35]. Although this hypothesis needs to be validated further by confirming the role of some of our
228 identified candidates as true disease initiation or progression factors in appropriate models of
229 infection, we emphasise the potential of *in vivo* transcriptomics at distinct stages of infection to detect
230 such initiation and progression factors, as has already been proposed [35].

231

232 *Validation of an identified gene, encoding a serine hydroxymethyltransferase (SHMT), as a promising*
233 *target for antifungal drug development.*

234 To demonstrate the value of the NanoString technology in identifying genes relevant for *A. fumigatus*
235 virulence, and aiming to validate a novel drug target, we decided to further investigate the serine
236 hydroxymethyltransferase encoding gene (*shmB,* AFUA_3G09320), which was consistently expressed
237 at higher levels *in vivo* compared with *in vitro* conditions (Fig. 1B). *A. fumigatus* genome encodes two
238 paralogues of serine hydroxymethyltransferase, ShmA (annotated as AFUA_2G07810, not included in
239 the NanoString analysis) and ShmB. The ShmB protein contains 471 amino acids (aa) and ShmA is 537
240 aa in length, and both share an identity of 61.9% and similarity of 79.9% (Fig. S3A). Interestingly, ShmA
241 has a long N-terminus region that is absent in ShmB (Fig. S3A), which prompted us to investigate the
242 subcellular localisation of the proteins using three different public softwares: DeepMito [36], PProwler
243 [37], and TargetP [38]. In contrast to the current annotation in FungiDB and NCBI databases, all three
244 algorithms predicted a mitochondrial localisation for ShmA and a cytosolic for ShmB. Indeed, when
245 we aligned the *A. fumigatus* proteins with their *Saccharomyces cerevisiae* orthologues, we observed
246 that the yeast mitochondrial enzyme SHM1 also had a longer N-terminus in comparison to the
247 cytosolic proteins (Fig. S3B).

248 Therefore, aiming to clarify the subcellular localisation of ShmA and ShmB in *A. fumigatus* we tagged
249 the proteins at their C-terminus with the fluorescent YFP-derivative Citrine to express them under the
250 control of their native promoters. In line with our predictions, we found that the ShmB-Citrine protein
251 localises throughout the cytoplasm, with a similar pattern to a control strain that expresses Citrine
252 under the control of the strong *gdpA* promoter (Fig. 4A). Regrettably, ShmA-Citrine could not be
253 detected, possibly reflecting very low or no expression of the encoding gene under steady-state
254 conditions, which would be supported by its dispensability under standard laboratory conditions (see
255 below).

256 To investigate the potential relevance of ShmA and ShmB for fungal virulence, we initially attempted
257 to construct single null mutants deleted for each encoding gene. We successfully constructed a *ΔshmA*
258 mutant, which showed no phenotype on regular laboratory conditions, growing perfectly on rich
259 Sabouraud and defined AMM media (Fig. S3C). In contrast, we were unable to generate a *ΔshmB*
260 mutant, suggesting that this might be an essential gene in *A. fumigatus*. We therefore constructed
261 two mutant strains in which we placed the *shmB* coding region under the control of the *tetOFF* module
262 [39, 40], one in the wild-type background and one in the *ΔshmA* background. The *tetOFF* system allows
263 downregulation of transcription of the gene of interest, in this case *shmB*, upon supplementation of
264 doxycycline (Dox) [39]. Addition of Dox inhibited growth of both strains (*shmB_tetOFF* and *ΔshmA-*
265 *shmB_tetOFF*) on AMM solid plates (Fig. 4B), proving that *shmB* is essential for viability independently
266 of its paralogue *shmA*. Gene essentiality is a conditional phenomenon, whereby particular
267 growth/environmental conditions may overcome the disturbances derived from the gene deficiency
268 [40-43]. Therefore, we attempted to reconstitute growth of the *shmB_tetOFF* strain in the presence
269 of Dox by supplementing compounds that could potentially be depleted in the absence of ShmB (Fig.
270 4C). We have previously observed that disturbances in the folate cycle causes a need of amino acid
271 supplementation [44], therefore, we assayed all phenotypic conditions on AMM without nitrogen
272 (AMM-N, to diversify and increase the presence of permeases in the membrane that ensure uptake
273 of amino acids and other compounds) supplemented with 1 mg/mL of all proteinogenic amino acids.
274 Additionally, we tried to reconstitute growth by supplementing the media with 5,10-
275 methylenetetrahydrofolate (CH_2-THF) and glycine (separately and combined), or with folic acid and
276 serine (substrates/products of the bidirectional enzymatic reaction), or with adenine (as blockade of
277 the folate cycle might impair purine biosynthesis [45]). In addition, we tested adding ATP to all those
278 supplements, as we previously showed that impairing the folate cycle *via* blocking the activity of
279 methionine synthase impacts cellular energetics in *A. fumigatus* [40]. The only condition that could
280 partly reconstitute growth, albeit not to wild-type levels, was supplementation with adenine and ATP
281 (Fig. 4C). None of the supplement combinations reconstituted growth of the *shmB_tetOFF* strain

282 under restrictive conditions (Fig. 4C). Therefore, either *shmB* is a truly essential gene, or the conditions
283 to overcome its essentiality are complex and yet unknown. Yet, based on these results *shmB*
284 constitutes a promising drug target candidate, and consequently we decided to test its value in an *in*
285 *vivo* infection model.

286 We have recently proposed that potential drug targets should be validated in models of established
287 infection, which is particularly relevant for essential genes (to confirm that essentiality cannot be
288 overcome during active growth in the host tissues) [40]. To this aim, we initially confirmed that Dox
289 addition very strongly turns down *shmB* expression in growing mycelium (Fig. S3D) and that this
290 downregulation causes a significant decrease in the growth capacity of 12h grown submerged mycelia,
291 as measured by fungal biomass (Fig. 4D). Therefore, we assayed our optimised protocol to investigate
292 targets in established *A. fumigatus* invasive pulmonary infections with the *tetOFF* system [40]. We
293 infected leukopenic mice with 2×10^5 conidia of the *shmB_tetOFF* strain, started Dox treatment 16h
294 after infection and measured fungal burden in the lungs 72h after infection. As control we also infected
295 mice with the previously validated strain *Δcyp51B-cyp51A-tetOFF* [40], which expresses *cyp51A*, the
296 gene that encodes the target of the azole antifungals, under the control of the same *tetOFF* system.
297 Therefore, this control strain serves to corroborate that downregulating a validated target (azoles are
298 the gold standard therapy for invasive pulmonary aspergillosis) causes a significant reduction in fungal
299 burden, as indeed we detected (Fig. 4E). Interestingly, we found that downregulation of *shmB* in the
300 established infection model triggered a significant reduction in fungal burden (Fig. 4E). Hence, ShmB
301 appears to be a valid target for the treatment of aspergillosis infections.

302

303 *Structural-based analysis of ShmB druggability*

304 The human serine hydroxymethyltransferase (SHMT) is considered a promising target for anti-cancer
305 drug development [46, 47] and accordingly various inhibitors have been already developed (for
306 instance, see references in [48]). Therefore, we decided to test the antifungal potential of one of such
307 inhibitors of the human SHMT, Hit-1 [49], on *A. fumigatus*. We performed broth microdilution assays
308 incubating the fungus in RPMI-1640 medium in the presence of increasing concentrations of Hit-1
309 (from 2 µg/mL=4.29 µM to 512 µg/mL=1.1 mM), and did not detect any antifungal activity of this
310 compound (Table 2). As this could be due to the incapacity of Hit-1 to penetrate fungal cells, we also
311 tested Hit-1 antifungal activity in the presence of colistin. This antibiotic has been shown to
312 permeabilise *Candida albicans* cells [50], and here we have confirmed that it also permeabilises *A.*
313 *fumigatus* swollen conidia to the membrane impermeable dyes FITC (fluorescein isothiocyanate) and

314 Zombie-Aqua (Fig. S4). However, Hit-1 did also not inhibit *A. fumigatus* growth in the presence of
315 colistin (Table 2).

	Minimum Inhibitory Concentration (MIC)
Colistin	> 64 µg/mL
Hit-1	> 512 µg/mL
Hit-1 + 2 µg/mL Colistin	> 512 µg/mL
Hit-1 + 4 µg/mL Colistin	> 512 µg/mL

316

317 **Table 2.** Broth microdilution assays of colistin and Hit-1 showed that neither of these compounds
318 inhibit growth at the tested concentrations.

319 As our previous results with the *tetOFF* promoter demonstrated that ShmB is essential for *A. fumigatus*
320 viability, we suspected that the inhibitor Hit-1, designed against the human enzyme, may not be
321 effective against the fungal enzyme. This led us to hypothesise that it should also be possible to design
322 fungal specific inhibitors, not active against the human enzyme. To substantiate this hypothesis our
323 initial step involved identifying the main druggable binding pocket of the human SHMT based on its
324 crystal structure as retrieved from the Protein Data Bank (accession number PDB ID 1bj4), using a
325 target-based *in silico* approach. We conducted two independent analyses employing the DrugRep [51]
326 and the PockDrug [52] engines. The PockDrug analysis yielded ten possible binding pockets, with only
327 six of them possessing a Druggability Probability score exceeding 0.5 (Fig. 5A). Cross-referencing with
328 the results from DrugRep revealed a single common pocket from both predictions: pocket A (Fig. 5A)
329 (Gln44 Ala383 Ile51 Glu374 Phe56 Ser381 Ala379 Glu69 Val46 Arg43 Cys384 Ala407 Gly47 Glu49 Ile382
330 Arg465 Glu378 Glu54 Asn55 Leu48). Next, we investigated whether this predicted binding pocket is
331 preserved in the *A. fumigatus* orthologue. To this purpose, we constructed a homological model of
332 the fungal protein using the *in silico* protein modelling AI AlphaFold [53]. Although the similarity
333 between the sequences is reasonably high (74.9%), indicating the protein is well preserved crossed
334 the species, there are some mutations in the amino acids within the key areas associated to the
335 hypothetical binding pocket (highlighted in red in Figure 5B). A close comparison revealed that such
336 mutations likely altered the conformation of the neighbouring amino acid residues hence resulting in
337 a different topology of pocket A compared to human SHMT, making it much shallower and smaller
338 (Figure 5C). In particular, the alteration in the position of Arg263 (Arg255 in *A. fumigatus* SHMT) has
339 formed a barrier resulting in the fungal pocket being almost half the size of the human pocket A.

340 Subsequently, we performed *in silico* docking using the SwissDock engine [54, 55] employing the Hit-
341 1 inhibitor (IC50 = 0.53 µM) [49] against pocket A of the human protein. This resulted in several
342 promising binding motifs occupying the entire pocket, as visually represented in Figure 5D. For
343 instance, in one of the top binding positions, HIT1.242 (ΔG = -7.57 kcal/mol; FullFitness = -2433.57
344 kcal/mol), Hit-1 nestled itself deep into the pocket, demonstrating hydrophobic interactions with the
345 pocket (Fig. 5E). Additionally, it also formed four hydrogen bonds distributed through the molecule
346 backbone (Ser`41, Gln`44, Arg`43 and Tip3`579; Fig. 5G), anchoring the ligand neatly into the pocket
347 (Fig. 5E). Subsequent *in silico* docking between Hit-1 and the fungal orthologue pocket A suggested
348 that Hit-1 could not bind as effectively. Only two binding motifs were suggested, both restricted to
349 the smaller *A. fumigatus* pocket (Figure 5D). Upon a closer inspection of the top binding motif, HIT1.28
350 (ΔG = -6.87 kcal/mol; FullFitness = -2143.87 kcal/mol; Fig. 5G), it is clear that the ligand is not
351 embedding deep into the pocket, indicating less hydrophobic interactions with the target. There is
352 only one hydrogen bond suggested between Hit-1 and the target (ASP`55; Fig. 5F), indicating a less
353 favourable binding compared to the human version of the protein. It also appeared that the altered
354 Arg255 indeed acted as a barrier, blocking Hit-1 from extending to the region proximal to Arg43 (Arg35
355 in *A. fumigatus* SHMT) and forming any additional hydrogen bonds (Fig. 5F). Therefore, it appears that
356 Hit-1 is specific to human SHMT as it cannot bind properly to the fungal orthologue, which would agree
357 with the observed absence of growth inhibition on *A. fumigatus* (Table 2). Similarly, we believe that
358 inhibitors that bind to the fungal, but not the human, enzyme pocket can be designed, and thus we
359 propose that the development of novel fungal-specific inhibitor agents against the promising SmhB
360 antifungal target is feasible.

361

362 **DISCUSION**

363 New antifungal agents are urgently needed, as resistance to the current drugs is widespread [56-58],
364 posing a great threat to human health [24]. In the endeavour of developing novel and efficient
365 chemotherapy, the selection of valid drug targets is crucial [59]. In the last few years, a variety of
366 innovative approaches have been applied to identify suitable target candidates. For instance,
367 comparative genomics [60], computer modelling [61], *in silico* analysis of protein interactions [62],
368 screening of deletion libraries [63], including competitive fitness assays [64], screening of regulatable
369 libraries [43, 65], construction of transposon insertion libraries [66, 67], or machine learning
370 approaches [68] have been employed to identify antifungal drug targets. In this regard, *in vivo*
371 transcriptomics has also been used frequently to understand fungal pathogenicity [34, 69-72], albeit
372 its potential to identify suitable antifungal targets still encounters some scepticism. In a seminal study,

373 McDonagh and colleagues [34] compared the transcriptome obtained from conidia germinating in
374 murine lungs with germlings obtained from *in vitro* conditions expected to match the *in vivo*
375 environment. This work could confirm that *A. fumigatus* encounters nutrient (particularly iron and
376 nitrogen) limitation as well as alkaline and oxidative stress during initiation of infection, providing
377 foundational cues about the conditions encountered by the fungal pathogen in the mammalian lung.
378 However, this study needed to use pools of 24 mice per sample, which limited the number of
379 conditions that could be tested (for instance, only one model of immunosuppression was assayed),
380 could only analysed the early initiation of infection (12-14 hours) and had to recover the fungal
381 material from bronchoalveolar lavages. These limitations were mainly due to the challenge of
382 recovering sufficient fungal RNA material from the infected tissue for the subsequent analysis. In a
383 more recent study, NanoString analysis was employed to identify *A. fumigatus* transcriptional factors
384 which are highly expressed or strongly up-regulated during growth in the murine lung tissues, and
385 experimentally proved that two of them are relevant in the context of infection [73]. Here we
386 reasoned that by comparing the transcription levels of genes related to sulfur metabolism in the
387 tissues versus a variety of *in vitro* S-sources could reveal gene products that are specifically
388 upregulated *in vivo*, and may therefore be relevant for the infection process and constitute promising
389 antifungal targets.

390 In our analysis of genes related with sulfur metabolism, we have identified 15 genes that are
391 consistently expressed at higher levels in the murine lungs than in all tested *in vitro* conditions. At
392 least 5 of those genes have been previously proven to be important for *A. fumigatus* virulence, and
393 additionally 6 genes have been suspected to be relevant as well (Table 1). We previously showed that
394 AFUA_5G02180, encoding cysteine synthase (CysB), is important for *A. fumigatus* virulence, as a
395 cysteine auxotroph had reduced virulence in a murine model of infection [14]. We have also
396 demonstrated that AFUA_8G04340 encodes cystathionine-γ-lyase (MecB), the major persulfidating
397 enzyme in *A. fumigatus*, which is relevant for fungal virulence [33]. The genes AFUA_2G07680,
398 encoding L-ornithine-*N* ^{5}-monooxygenase (SidA), which catalyses the first committed step of
399 siderophore biosynthesis, and AFUA_5G03920, encoding the master transcriptional regulator for
400 adaptation to iron limitation (HapX), have been shown to be crucial for virulence [28, 29]. Finally, the
401 gene AFUA_8G04340, encoding the transcriptional activator of the cross-pathway control system of
402 amino acid biosynthesis (CpcA), was also reported to contribute to *A. fumigatus* virulence [30].
403 Therefore, we propose that the remaining genes are also likely to be important for *A. fumigatus*
404 virulence and thus constitute good candidates to validate experimentally. It is noteworthy that genes
405 that we have characterized and shown to be dispensable for virulence (AFUA_1G05020 -*sB*- and
406 AFUA_2G15590 -*sF*- [14]) were not detected in this analysis, further supporting the hypothesis that

407 the genes identified may indeed be relevant. Nevertheless, it also needs to be mentioned that several
408 genes that have been described as relevant for virulence in other studies were not identified as
409 universally important in our analysis (for instance, AFUA_6G04700 -HisB- , AFUA_4G06530 -MetR- or
410 AFUA_2G14210 - Ilv3A/IlvC- [13, 26, 74]), implying that our approach is not able to detect all genes
411 relevant for infection. Yet, our analysis has identified some of these genes as potential disease
412 initiation or progression factors, which opens the question of whether their relevance for infection
413 might be time-dependent.

414 In fact, our temporal analysis has revealed various potential disease initiation and progression factors.
415 These are defined as products that are required for the initiation of infection or for the persistence
416 and progression of disease [35]. Differentiating these actions is paramount for drug discovery, as it
417 would not be adequate to develop a drug to treat established infections that targets an initiation
418 factor, and similarly, it would not be appropriate using a drug that targets a progressing factor as
419 prophylaxis. Therefore, discerning disease initiation and progression factors would be important to
420 better understand the infective capacity of *A. fumigatus* and to expand our reservoir of potential
421 antifungal targets. In fact, progression factors, which are usually not identified in classic virulence
422 studies, are regarded as valuable targets, as antimicrobials are often employed to treat established
423 infection [35]. In this respect, we previously negated a role of *sFα* (AFUA_6G08920) and *sB*
424 (AFUA_1G05020) in *A. fumigatus* virulence by infecting leukopenic mice with null mutants [14], but
425 our current results suggest that they might be disease progression factors specifically relevant in the
426 steroid model (Fig. 3C).

427 It was unfortunate that the samples from two leukopenic mice did not run properly and had to be
428 excluded from the analyses. We acknowledge that this limits the value of some of our results,
429 particularly the comparisons among time-points and the analysis of temporal expression of genes in
430 leukopenic mice. However, as all the infections for the *in vivo* samples of the analysis were carried out
431 simultaneously, we reasoned that repeating just two mice would not provide fully consistent results.
432 Indeed, we tried to include the data obtained from the two leukopenic mice of the preliminary
433 experiment to validate the linear amplification protocol (Fig. 1A), but found that these samples
434 clustered slightly separated from the other *in vivo* samples (Fig S5), and therefore could not be used
435 for the model and temporal analyses. Importantly, including these two mice, the overall profile of
436 expression relative to *in vitro* remained highly similar, such that the 15 genes previously detected to
437 be consistently upregulated *in vivo* VS *in vitro* were still detected (Fig. S5), which shows the strength
438 of the results. In addition, with these two additional mice one more gene was included in the list of
439 candidates, AFUA_5G07210. This gene encodes a homoserine O-acetyltransferase, which has been
440 described as important for virulence in the fungal pathogen *Cryptococcus neoformans* [75].

441 One of the uncharacterised genes in our list of 15 potentially relevant genes encodes a serine
442 hydroxymethyltransferase (SHMT). SHMT is a pyridoxal phosphate-dependent enzyme of the folate
443 cycle that catalyses the reversible conversion of serine and tetrahydrofolate (THF) into glycine and
444 5,10-methylenetetrahydrofolate (CH_2-THF). Fungi encode two isoforms in the nuclear genome, one
445 cytosolic and one mitochondrial [45]. In *S. cerevisiae* both genes were disrupted singly and in
446 combination, generating auxotrophic viable strains [76]. In contrast to our results, the deletant of the
447 cytosolic SHMT encoding gene (*SHM2*) grew well in the presence of the substrates glycine and
448 formate. In addition, the cytosolic and mitochondrial SHMT encoding genes could also be deleted in
449 the ascomycete *Ashbya gossypii* [77], where supplementation with adenine or glycine could
450 reconstitute growth of the cytosolic *SHMT* (*SHM2*) knock out. Therefore, essentiality of the cytosolic
451 ShmB in *A. fumigatus* suggests that the metabolic implications of disrupting the one carbon-cycle are
452 more complex in this pathogen than in other fungi. Indeed, we previously showed that in contrast to
453 other fungi, the absence of methionine synthase, which forms a junction between the one carbon
454 cycle and the trans-sulfuration pathway, causes an imbalance in cell energetics, possibly initiated by a
455 cellular sensing of purine depletion, that halts fungal growth [40]. Here we found that adenine could
456 partly reconstitute growth of the *shmB_tetOFF* strain in restrictive conditions, which resembles the
457 phenotype we observed with *metH_tetOFF* [40]; but in contrast to the absence of MetH, ATP could
458 not fully reconstitute growth in the absence of ShmB, reflecting that we do not understand the
459 metabolic implications of eliminating the cytosolic serine hydroxymethyltransferase activity. Given its
460 essentiality, we hypothesised that it could constitute a good target for the development of novel
461 antifungals, and indeed we have validated it in a murine model of established infection using the
462 *tetOFF* system. To our knowledge the relevance of serine hydroxymethyltransferases for fungal
463 pathogenicity had not been investigated before. In contrast, this enzyme has been shown to be a
464 promising antimalarial target [78] and implicated in a variety of virulence related traits in bacteria. For
465 instance, a null mutant in *Staphylococcus aureus* showed impaired survival inside macrophages and
466 reduced virulence in a *Galleria mellonella* infection model [79]. In *Helicobacter pylori*, deletion of the
467 SHMT encoding gene *glyA* caused reduced growth rate [80], and in *Pseudomonas aeruginosa* controls
468 rugose colony morphology, increases biofilm formation, abolishes swarming and relates to the redox
469 status of the cells and the control of iron acquisition [81]. Therefore, targeting microbial SMHT
470 enzymes seems to be a promising antimicrobial strategy. Nevertheless, as the current SHMT inhibitors
471 have been developed against the human enzyme, specific inhibitors against the microbial proteins
472 need to be designed. By comparing the pocket landscape of the *A. fumigatus* and human enzymes and
473 performing a docking assay with a known inhibitor of the human SHMT, here we show that there are
474 sufficient differences to pursue the development of a fungal specific agent. A comparable situation

475 occurs in the case of efforts to inhibit the promising antifungal target calcineurin. The human and
476 fungal enzymes are highly similar, such that in this case a drug developed against the human protein
477 (FK506) can inhibit the fungal enzyme and is a potent antifungal agent. Fuelled by structural insight,
478 recent research is focused on developing FK506 fungal specific derivatives, which has already
479 generated promising results [82-84].

480 In conclusion, in this study we show that *in vivo* transcriptomics is a valid strategy to identify virulence
481 traits in *A. fumigatus*. Using the NanoString technology we have detected 15 genes as potentially
482 relevant for pathogenicity, five of which have already been proven experimentally. We further
483 investigate one novel gene, encoding the cytosolic serine hydroxymethyltransferase, thereby
484 demonstrating that this is an essential gene product for *A. fumigatus* viability and virulence, and that
485 it seems possible to design specific inhibitors for the fungal enzyme. Therefore, we have validated
486 cSHMT as a promising antifungal target for future research efforts.

487

488 **MATERIAL AND METHODS**

489 *Fungal strains and culture media*

490 The *Aspergillus fumigatus* strain ATCC46645 [85] was used for the transcriptomic analysis, and the
491 MFIG001 isolate (*ΔKU80*) for genetic manipulation [86]. The strains were routinely grown on
492 Sabouraud solid medium (Oxoid) for 3-5 days at 37 °C for spore harvesting.

493 For phenotyping analysis, the isolates were inoculated on solid *Aspergillus* Minimal Medium (AMM,
494 1% glucose, 5 mM ammonium tartrate, 7 mM KCl, 11 mM KH_2PO_4, 0.25 mM $MgSO_4$, 1× Hutner's trace
495 elements solution [pH 5.5], 1.5% agar), supplemented as indicated in each section, and incubated at
496 37 °C for 2-3 days. Phenotypic experiments were performed at least twice independently.

497 For selection in the presence of resistance markers 50 µg ml^{-1} of hygromycin B or 100 µg ml^{-1} of
498 pyrithiamine (InvivoGen) were added to the AMM in the growth plates.

499

500 *Mutant construction*

501 To generate the *ΔshmA* mutant and attempt to construct the *ΔshmB* mutant, we followed a previously
502 optimised protocol [87]. Briefly, upstream and downstream fragments of the genes were amplified by
503 HIFI-PCR and fused to the Hygromycin-B (*hph*) selective cassette by fusion PCR. This deletant cassette
504 was used to replace the target gene by homologous recombination in the *ΔKU80* strain MFIG001.

505 To construct the *shmB_tetOFF* isolate, we followed CRISPR-Cas9 mediated recombination, as
506 previously described for *A. fumigatus* [88]. Briefly, a repair template containing the *tetOFF* module
507 and a pyrithiamine resistance marker (PtrA), was amplified from pSK606 [39] using Phusion green hot
508 start II high-fidelity PCR master mix (ThermoFisher Scientific). The repair template had 50 bp flanking
509 regions homologous to the upstream and downstream sequences at the ATG start codon, placing the
510 *tetOFF* module immediately 5'- of the *shmB* ORF. The sequence of the targeted gRNA (crRNA) was
511 (GTCCAAATGAAAGAAAACAA|TGG) and was designed using EuPaGDT [89].

512 To construct the fluorescent SHMT strains, we inserted the correspondent repair template, containing
513 Citrine and the pyrithiamine resistance marker, at the 3'-UTR of each gene using CRISPR-Cas9 as
514 previously descried [88]. Each repair template carried flanking homology regions to the targeted gene.
515 The targeted gRNAs used were (5'-GACAGGCAGGGGGTAGGTGC-3') and (5'-
516 GGGCACTTTCAGCCTTCCGT-3') for *shmB* and *shmA*, respectively.

517 All primers used in the study can be found in Table S3.

518

519 *Localisation studies of ShmB-Citrine*

520 *A. fumigatus* conidia were inoculated in 200 µL of filtered autoclaved AMM on 8 well chambers slides
521 (IBIDI) and incubated at 30 °C for 16h. Imagining was performed using a Leica SP8x laser scanning
522 confocal microscope equipped with a 63x (NA 1.4) HC PLAN APO CS2 oil immersion objective. The
523 pinhole was set to one Airy unit and the gain was set to 200. To visualise the localisation of labelled
524 proteins, fluorescence imaging was performed using an excitation of 516 nm and 529 nm emission
525 using a white light laser. Image format captures was 1024x1024 at 400 hz scan speed. Z-stacks of
526 germlings were taken at 1.0 microns and slices were projected as average intensity using ImageJ no
527 adjustments to brightness or contrast were made. Scale bars are shown.

528

529 *Murine Infections*

530 Mouse infections experiments were performed under United Kingdom Home Office project license
531 PDF8402B7 and approved by the University of Manchester Ethics Committee and by the Biological
532 Services Facility at the Faculty of Biology, Medicine and Health, University of Manchester.

533 Outbred CD1 male mice (22 to 26 g) were purchased from Charles Rivers and left to rest for at least
534 one week before the experiment. Mice were allowed access *ad libitum* to water and food throughout
535 the experiment.

536 For the leukopenic model mice were immunosuppressed with 150 mg/kg of cyclophosphamide
537 (Baxter) on days −3 and −1 plus 1 subcutaneous injection of 250 mg/kg hydrocortisone 21-Acetate
538 (Sigma-Aldrich) on day −1. For the corticosteroid model, mice were injected with a single dose of 40
539 mg/kg of triamcinolone (Bristol Myers Squibb) on day −1. Bacterial infections were prevented by
540 adding 2 g/L neomycin to the drinking water. Mice were anesthetized by exposure to 2% to 3%
541 isoflurane (Sigma-Aldrich) for 5 to 10 minutes and intranasally infected with 40 µL of a suspension
542 containing 10^5 spores for the leukopenic model and 10^6 spores for the corticosteroid model. For both
543 models, 3 mice per time point post infection (16, 24 or 72h) were used. At the designated time-points,
544 mice were sacrificed by a lethal injection of pentobarbital and the lungs were harvested to be
545 immediately snap frozen for RNA isolation.

546 For the chronic model, we followed a published protocol [25, 90]. Briefly, an immunocompetent
547 mouse was anesthetised by intraperitoneal injection of a ketamine (1%)/xylazine (0,2%) solution and
548 intratracheally inoculated with 50 µL of a suspension of agar beads containing 5×10^7 conidia/mL.
549 Infection was left to progress for 21 days before the mouse was sacrificed for further processing.

550 To monitor virulence of the *shmB_tetOFF* strain, we followed our previously optimised protocol [40].
551 Briefly, groups of 10 mice were infected with 40 µL of a suspension containing 2×10^5 of the
552 *shmB_tetOFF* or the control *Δcyp51B-cyp51A-tetOFF* strain (inocula were confirmed by plating
553 dilutions of the used suspensions). Five mice per strain received doxycycline (Dox) treatment and five
554 PBS vehicle. Dox treatment started 16h after infection by an intraperitoneal injection (50 mg/kg) and
555 change to Dox-containing food (Envingo Safe-Diet U8200 version 0115 A03 0.625 g/kg Doxycycline
556 Hyclate pellets). Treatment was maintained by subcutaneous 50 mg/kg Dox injections every 12h post
557 infection until the end of the experiment after 72h.

558

559 *NanoString analysis: Preparation of samples, hybridisation and data processing*

560 RNA from *in vitro* conditions was isolated as previously described [13]. Briefly, mycelia were shifted
561 from a culture grown overnight in AMM to new flasks containing the defined sources described in
562 Table S2. Mycelia were incubated for 4h in the new conditions, then filtrated trough sterile Miracloth
563 (Merck Millipore) and snap frozen in liquid nitrogen. Mycelia were ground in the constant presence of
564 liquid nitrogen and RNA was isolated using the RNeasy Plant Mini Kit (Qiagen) following the
565 manufacturer's instructions and including the on column DNAse digestion step. RNA was assessed by
566 a NanoDrop 2000 spectrophotometer (Thermo Fisher Scientific) to determine quality and
567 concentration.

568 RNA from murine lungs was isolated as follows: Lungs were lyophilized for 48h in a CoolSafe ScanVac
569 freeze drier connected to a VacuuBrand pump and subsequently ground in the presence of liquid
570 nitrogen. The resulting powder was resuspended in TRIzol reagent (Invitrogen – Thermofisher) and
571 processed following the manufacturer's instructions. RNA was cleaned with
572 Phenol:Chloroform:Isoamyl (25:24:1) (Sigma) and extracted with Chloroform (Invitrogen).
573 Subsequently, RNA was purified using the RNeasy Minikit (Qiagen), following the clean-up protocol,
574 and including the on column DNAse digestion step.

575 RNA isolated from murine lungs was subjected to the NanoString nCounter Single Cell Gene Expression
576 protocol for linear amplification of target genes. Briefly, RNA was converted to cDNA using SuperScript
577 VILO MasterMix (Life Technologies). To confirm that target RNA was present in the samples, and that
578 cDNA has been properly generated, a Real-Time PCR was performed using the gene AFUA_4G07360
579 (*metH*) as target, as a RT-PCR for this transcript had been validated before [40]. Genes of interest were
580 linearly amplified using the Multiplex Target Enrichment (MTE) primers (Supplementary File 1) and a
581 PCR protocol consisting of 16 MTE amplification cycles of 94°C 15 seconds and 60°C 4 minutes, with
582 the TaqMan PreAmp Master Mix (Life Technologies).

583 cDNA samples were incubated for 2 minutes at 94°C and then snap cool on ice prior to addition to the
584 hybridization reaction. Hybridization was performed according to the Elements Tagset Hybridisation
585 setup, as detailed by Nanostring and using the NanoString custom designed probes A and B
586 (Supplementary File 1). The cartridge was read using the flex system, consisting of nCounter Prep
587 Station and the Digital Analyser.

588 The saw data file (Supplementary File S2) was initially subjected to a Quality Control check. This
589 consisted of the monitorization of the counts of the internal positive control (positive performance
590 for hybridization verification) and the total counts detected for each of the conditions (Fig. S1).

591 Raw data (Supplementary File 2) was normalised using the nSolver 4.0 software (NanoString). Data
592 was first subjected to Background Subtraction using the geometric mean of the negative control
593 counts. Subsequently, data was normalized using both the geometric mean of positive control count
594 and the geometric mean of the housekeeping genes (Supplementary File 3).

595 Normalised data was analysed using the Agglomerative Cluster – Heat map option of the nSolver 4.0
596 software (NanoString). Spearman Correlation was used as distance metric and Average was used as
597 linkage method.

598

599

600 *Computational structure analyses*

601 The crystal structure of the serine hydroxymethyltransferase (SHMT) was obtained from Research
602 Collaboratory for Structural Bioinformatics Protein Data Bank (RCSB PDB, http://www.rcsb.org) in PDB
603 format, referenced by its protein data bank ID 1bj4. The structure of the fungal SHMT was predicted
604 using AlphaFold2 [53]. The amino acid sequence was retrieved from FungiDatabase [91] and utilised
605 as input, with the highest scoring model (pLDDT= 96.9, pTMscore= 0.943) selected for downstream *in*
606 *silico* analysis.

607 For the human SHMT, DrugRep [51] and PockDrug [52] were employed for target based binding pocket
608 prediction. DrugRep is a receptor-based screening tool utilising CB-Dock to identify docking pockets
609 of the protein receptor. PockDrug utilizes the fpocket estimation method, based on holo or apo
610 proteins, for predicted pocket estimation. This method involves preliminary detection of cavities
611 capable of binding a ligand of sufficient size, though without ligand proximity information. Pockets
612 with a predicted druggability score above 0.5 from DrugRep were recorded and cross-referenced with
613 suggestions from PockDoc to determine the 'optimal' binding pocket for subsequent *in-silico* docking.

614 Ligand Hit-1 was drawn using Marvin JS (https://marvinjs-demo.chemaxon.com/latest/demo.html
615 [92]). The binding mode of Hit-1 to optimal binding pocket in SHMT was predicted using the EADock
616 DS based SwissDock (http://www.swissdock.ch/docking# [55]). The binding modes with the most
617 favourable energies were evaluated with FACTS (Fast Analytical Continuum Treatment of Solvation
618 [93]) and then output as clusters. The best docking pose, exhibiting maximal hydrophobicity pockets
619 coverage and hydrogen bonding, was manually selected. Outputs from all programmes were
620 visualised in PyMOL 2.5 (Schrödinger, LLC).

621

622 **ACKOWLEDGEMENTS**

623 We would like to specially thank Prof Sven Krappmann, who guided JA to discover the NanoString
624 technology some years ago and so inspired this work. In addition, we would like to thank Emilia
625 Mellado and Sven Krappmann for critical reading of the manuscript. We acknowledge the use of the
626 Genomic Technologies Facility (Faculty of Biology Medicine and Health, University of Manchester) for
627 the NanoString hybridisation and data read. Help and support from members of the Manchester
628 Fungal Infection Group (MFIG) and the Spanish National Centre for Mycology (LRIM) is greatly
629 appreciated.

R. Alharthi was funded by the Ministry of Education of Saudi Arabia. J Amich was funded by an MRC Career Development Award (MR/N008707/1). M. Bromley was supported by Wellcome Trust (grants: 219551/Z/19/Z and 208396/Z/17/Z).

633 **REFERENCES**

634 1. Tekaia, F. and J.P. Latge, *Aspergillus fumigatus: saprophyte or pathogen?* Curr Opin Microbiol,
635 2005. **8**(4): p. 385-92.
636 2. Hospenthal, D.R., K.J. Kwon-Chung, and J.E. Bennett, *Concentrations of airborne Aspergillus*
637 *compared to the incidence of invasive aspergillosis: lack of correlation.* Med Mycol, 1998.
638 **36**(3): p. 165-8.
639 3. Latge, J.P., *Aspergillus fumigatus and aspergillosis.* Clin Microbiol Rev, 1999. **12**(2): p. 310-50.
640 4. Park, S.J. and B. Mehrad, *Innate Immunity to Aspergillus Species.* Clinical Microbiology
641 Reviews, 2009. **22**(4): p. 535-551 DOI: 10.1128/cmr.00014-09.
642 5. Kosmidis, C. and D.W. Denning, *The clinical spectrum of pulmonary aspergillosis.* Thorax, 2015.
643 **70**(3): p. 270-7 DOI: 10.1136/thoraxjnl-2014-206291.
644 6. Lowes, D., et al., *Predictors of mortality in chronic pulmonary aspergillosis.* Eur Respir J, 2017.
645 **49**(2) DOI: 10.1183/13993003.01062-2016.
646 7. Brown, G.D., et al., *Hidden killers: human fungal infections.* Sci Transl Med, 2012. **4**(165): p.
647 165rv13 DOI: 10.1126/scitranslmed.3004404.
648 8. Lestrade, P.P., et al., *Voriconazole Resistance and Mortality in Invasive Aspergillosis: A*
649 *Multicenter Retrospective Cohort Study.* Clin Infect Dis, 2019. **68**(9): p. 1463-1471 DOI:
650 10.1093/cid/ciy859.
651 9. Meis, J.F., et al., *Clinical implications of globally emerging azole resistance in Aspergillus*
652 *fumigatus.* Philos Trans R Soc Lond B Biol Sci, 2016. **371**(1709) DOI: 10.1098/rstb.2015.0460.
653 10. Scott, J. and J. Amich, *Primary Metabolism of Human Pathogenic Fungi, Importance for*
654 *Virulence and Potential for Drug Development*, in *Encyclopedia of Infection and Immunity*.
655 2022. p. 377-407.
656 11. Ene, I.V., et al., *Metabolism in Fungal Pathogenesis.* Cold Spring Harbor Perspectives in
657 Medicine, 2014. **4**(12): p. a019695-a019695 DOI: 10.1101/cshperspect.a019695.
658 12. Amich, J., S. Krappmann, and A.K. Bachhawat, *Editorial: Sulphur Metabolism of Fungi -*
659 *Implications for Virulence and Opportunities for Therapy.* Frontiers in Microbiology, 2020. **11**
660 DOI: 10.3389/fmicb.2020.583689.
661 13. Amich, J., et al., *Regulation of sulphur assimilation is essential for virulence and affects iron*
662 *homeostasis of the human-pathogenic mould Aspergillus fumigatus.* PLoS Pathog, 2013. **9**(8):
663 p. e1003573 DOI: 10.1371/journal.ppat.1003573.
664 14. Amich, J., et al., *Exploration of Sulfur Assimilation of Aspergillus fumigatus Reveals*
665 *Biosynthesis of Sulfur-Containing Amino Acids as a Virulence Determinant.* Infect Immun,
666 2016. **84**(4): p. 917-29 DOI: 10.1128/IAI.01124-15.
667 15. Scott, J., et al., *Targeting Methionine Synthase in a Fungal Pathogen Causes a Metabolic*
668 *Imbalance That Impacts Cell Energetics, Growth, and Virulence.* mBio, 2020. **11**(5) DOI:
669 10.1128/mBio.01985-20.
670 16. Traynor, A.M., et al., *Involvement of Sulfur in the Biosynthesis of Essential Metabolites in*
671 *Pathogenic Fungi of Animals, Particularly Aspergillus spp.: Molecular and Therapeutic*
672 *Implications.* Frontiers in Microbiology, 2019. **10** DOI: 10.3389/fmicb.2019.02859.
673 17. Bachhawat, A.K. and A.K. Yadav, *Metabolic Pathways as Drug Targets: Targeting the Sulphur*
674 *Assimilatory Pathways of Yeast and Fungi for Novel Drug Discovery*, in *Combating Fungal*
675 *Infections*. 2010. p. 327-346.
676 18. Kuplińska, A. and K. Rząd, *Molecular targets for antifungals in amino acid and protein*
677 *biosynthetic pathways.* Amino Acids, 2021. **53**(7): p. 961-991 DOI: 10.1007/s00726-021-
678 03007-6.
679 19. Xu, W., et al., *Pathogen Gene Expression Profiling During Infection Using a Nanostring*
680 *nCounter Platform*, in *Yeast Functional Genomics*. 2016. p. 57-65.

20. Bourré, L., *Genome-Wide RNAseq and Array-Based NanoString Transcriptomic Technologies: Which To Use and When? - Crown Bioscience*. 2020: https://blog.crownbio.com/genome-wide-rnaseq-and-array-based-nanostring-transcriptomic-technologies.
21. Veldman-Jones, M.H., et al., *Evaluating Robustness and Sensitivity of the NanoString Technologies nCounter Platform to Enable Multiplexed Gene Expression Analysis of Clinical Samples.* Cancer Research, 2015. **75**(13): p. 2587-2593 DOI: 10.1158/0008-5472.Can-15-0262.
22. Geiss, G.K., et al., *Direct multiplexed measurement of gene expression with color-coded probe pairs.* Nature Biotechnology, 2008. **26**(3): p. 317-325 DOI: 10.1038/nbt1385.
23. Fisher, M.C., et al., *Tackling the emerging threat of antifungal resistance to human health.* Nature Reviews Microbiology, 2022. **20**(9): p. 557-571 DOI: 10.1038/s41579-022-00720-1.
24. Fisher, M.C., et al., *Worldwide emergence of resistance to antifungal drugs challenges human health and food security.* Science, 2018. **360**(6390): p. 739-742 DOI: 10.1126/science.aap7999.
25. Urb, M., et al., *Evolution of the Immune Response to Chronic Airway Colonization with Aspergillus fumigatus Hyphae.* Infection and Immunity, 2015. **83**(9): p. 3590-3600 DOI: 10.1128/iai.00359-15.
26. Dietl, A.-M., et al., *Histidine biosynthesis plays a crucial role in metal homeostasis and virulence of Aspergillus fumigatus.* Virulence, 2016. **7**(4): p. 465-476 DOI: 10.1080/21505594.2016.1146848.
27. Wangsanut, T. and M. Pongpom, *The Role of the Glutathione System in Stress Adaptation, Morphogenesis and Virulence of Pathogenic Fungi.* International Journal of Molecular Sciences, 2022. **23**(18) DOI: 10.3390/ijms231810645.
28. Schrettl, M., et al., *HapX-mediated adaption to iron starvation is crucial for virulence of Aspergillus fumigatus.* PLoS Pathog, 2010. **6**(9): p. e1001124.
29. Schrettl, M., et al., *Siderophore biosynthesis but not reductive iron assimilation is essential for Aspergillus fumigatus virulence.* J Exp Med, 2004. **200**(9): p. 1213-9.
30. Krappmann, S., et al., *The Aspergillus fumigatus transcriptional activator CpcA contributes significantly to the virulence of this fungal pathogen.* Mol Microbiol, 2004. **52**(3): p. 785-99.
31. Liu, T.-B. and C. Xue, *The Ubiquitin-Proteasome System and F-box Proteins in Pathogenic Fungi.* Mycobiology, 2018. **39**(4): p. 243-248 DOI: 10.5941/myco.2011.39.4.243.
32. Jöhnk, B., et al., *SCF Ubiquitin Ligase F-box Protein Fbx15 Controls Nuclear Co-repressor Localization, Stress Response and Virulence of the Human Pathogen Aspergillus fumigatus.* PLOS Pathogens, 2016. **12**(9) DOI: 10.1371/journal.ppat.1005899.
33. Sueiro-Olivares, M., et al., *Fungal and host protein persulfidation are functionally correlated and modulate both virulence and antifungal response.* PLOS Biology, 2021. **19**(6) DOI: 10.1371/journal.pbio.3001247.
34. McDonagh, A., et al., *Sub-telomere directed gene expression during initiation of invasive aspergillosis.* PLoS Pathog, 2008. **4**(9): p. e1000154 DOI: 10.1371/journal.ppat.1000154.
35. Cramer, R.A. and C.H. Kowalski, *Is It Time To Kill the Survival Curve? A Case for Disease Progression Factors in Microbial Pathogenesis and Host Defense Research.* mBio, 2021. **12**(1) DOI: 10.1128/mBio.03483-20.
36. Savojardo, C., et al., *DeepMito: accurate prediction of protein sub-mitochondrial localization using convolutional neural networks.* Bioinformatics, 2020. **36**(1): p. 56-64 DOI: 10.1093/bioinformatics/btz512.
37. Hawkins, J. and M. BodÉN, *Detecting and Sorting Targeting Peptides with Neural Networks and Support Vector Machines.* Journal of Bioinformatics and Computational Biology, 2011. **04**(01): p. 1-18 DOI: 10.1142/s0219720006001771.
38. Almagro Armenteros, J.J., et al., *Detecting sequence signals in targeting peptides using deep learning.* Life Science Alliance, 2019. **2**(5) DOI: 10.26508/lsa.201900429.
39. Wanka, F., et al., *Tet-on, or Tet-off, that is the question: Advanced conditional gene expression in Aspergillus.* Fungal Genet Biol, 2016. **89**: p. 72-83 DOI: 10.1016/j.fgb.2015.11.003.

731 40. Scott, J., et al., *Targeting Methionine Synthase in a Fungal Pathogen Causes a Metabolic*
732 *Imbalance That Impacts Cell Energetics, Growth, and Virulence.* mBio, 2020. **11**(5) DOI:
733 10.1128/mBio.01985-20.
734 41. Beattie, S.R., et al., *Filamentous fungal carbon catabolite repression supports metabolic*
735 *plasticity and stress responses essential for disease progression.* PLoS Pathog, 2017. **13**(4): p.
736 e1006340 DOI: 10.1371/journal.ppat.1006340.
737 42. Cramer, R.A., *In vivo veritas: Aspergillus fumigatus proliferation and pathogenesis--*
738 *conditionally speaking.* Virulence, 2016. **7**(1): p. 7-10 DOI: 10.1080/21505594.2015.1134074.
739 43. Hu, W., et al., *Essential Gene Identification and Drug Target Prioritization in Aspergillus*
740 *fumigatus.* PLoS Pathogens, 2007. **3**(3) DOI: 10.1371/journal.ppat.0030024.
741 44. Scott, J., et al., *Pseudomonas aeruginosa-Derived Volatile Sulfur Compounds Promote Distal*
742 *Aspergillus fumigatus Growth and a Synergistic Pathogen-Pathogen Interaction That Increases*
743 *Pathogenicity in Co-infection.* Front Microbiol, 2019. **10**: p. 2311 DOI:
744 10.3389/fmicb.2019.02311.
745 45. Cossins, E.A. and L. Chen, *Folates and one-carbon metabolism in plants and fungi.*
746 Phytochemistry, 1997. **45**(3): p. 437-452 DOI: 10.1016/s0031-9422(96)00833-3.
747 46. Jain, M., et al., *Metabolite Profiling Identifies a Key Role for Glycine in Rapid Cancer Cell*
748 *Proliferation.* Science, 2012. **336**(6084): p. 1040-1044 DOI: 10.1126/science.1218595.
749 47. Paone, A., et al., *SHMT1 knockdown induces apoptosis in lung cancer cells by causing uracil*
750 *misincorporation.* Cell Death Dis, 2014. **5**(11): p. e1525 DOI: 10.1038/cddis.2014.482.
751 48. Scaletti, E., et al., *Structural basis of inhibition of the human serine hydroxymethyltransferase*
752 *SHMT2 by antifolate drugs.* FEBS Letters, 2019. **593**(14): p. 1863-1873 DOI: 10.1002/1873-
753 3468.13455.
754 49. Nonaka, H., et al., *Design strategy for serine hydroxymethyltransferase probes based on retro-*
755 *aldol-type reaction.* Nature Communications, 2019. **10**(1) DOI: 10.1038/s41467-019-08833-7.
756 50. Bibi, M., et al., *Combining Colistin and Fluconazole Synergistically Increases Fungal Membrane*
757 *Permeability and Antifungal Cidality.* ACS Infectious Diseases, 2021. **7**(2): p. 377-389 DOI:
758 10.1021/acsinfecdis.0c00721.
759 51. Gan, J.-h., et al., *DrugRep: an automatic virtual screening server for drug repurposing.* Acta
760 Pharmacologica Sinica, 2022. **44**(4): p. 888-896 DOI: 10.1038/s41401-022-00996-2.
761 52. Hussein, H.A., et al., *PockDrug-Server: a new web server for predicting pocket druggability on*
762 *holo and apo proteins.* Nucleic Acids Research, 2015. **43**(W1): p. W436-W442 DOI:
763 10.1093/nar/gkv462.
764 53. Jumper, J., et al., *Highly accurate protein structure prediction with AlphaFold.* Nature, 2021.
765 **596**(7873): p. 583-589 DOI: 10.1038/s41586-021-03819-2.
766 54. Grosdidier, A., V. Zoete, and O. Michielin, *Fast docking using the CHARMM force field with*
767 *EADock DSS.* J Comput Chem, 2011. **32**(10): p. 2149-59 DOI: 10.1002/jcc.21797.
768 55. Grosdidier, A., V. Zoete, and O. Michielin, *SwissDock, a protein-small molecule docking web*
769 *service based on EADock DSS.* Nucleic Acids Res, 2011. **39**(Web Server issue): p. W270-7 DOI:
770 10.1093/nar/gkr366.
771 56. Lestrade, P.P.A., et al., *Triazole resistance in Aspergillus fumigatus: recent insights and*
772 *challenges for patient management.* Clinical Microbiology and Infection, 2019. **25**(7): p. 799-
773 806 DOI: 10.1016/j.cmi.2018.11.027.
774 57. Pristov, K.E. and M.A. Ghannoum, *Resistance of Candida to azoles and echinocandins*
775 *worldwide.* Clinical Microbiology and Infection, 2019. **25**(7): p. 792-798 DOI:
776 10.1016/j.cmi.2019.03.028.
777 58. Zafar, H., et al., *A titanic drug resistance threat in Cryptococcus neoformans.* Current Opinion
778 in Microbiology, 2019. **52**: p. 158-164 DOI: 10.1016/j.mib.2019.11.001.
779 59. Mota Fernandes, C., et al., *The Future of Antifungal Drug Therapy: Novel Compounds and*
780 *Targets.* Antimicrobial Agents and Chemotherapy, 2021. **65**(2) DOI: 10.1128/aac.01719-20.

60. Abadio, A.K.R., et al., *Comparative genomics allowed the identification of drug targets against human fungal pathogens.* BMC Genomics, 2011. **12**(1) DOI: 10.1186/1471-2164-12-75.
61. Bencurova, E., et al., *Identification of Antifungal Targets Based on Computer Modeling.* Journal of Fungi, 2018. **4**(3) DOI: 10.3390/jof4030081.
62. Chaudhary, R., et al., *In Silico Protein Interaction Network Analysis of Virulence Proteins Associated with Invasive Aspergillosis for Drug Discovery.* Current Topics in Medicinal Chemistry, 2019. **19**(2): p. 146-155 DOI: 10.2174/1568026619666181120150633.
63. Noble, S.M., et al., *Systematic screens of a Candida albicans homozygous deletion library decouple morphogenetic switching and pathogenicity.* Nature Genetics, 2010. **42**(7): p. 590-598 DOI: 10.1038/ng.605.
64. van Rhijn, N., et al., *Functional analysis of the Aspergillus fumigatus kinome identifies a druggable DYRK kinase that regulates septal plugging.* Nature Communications, 2024. **15**(1) DOI: 10.1038/s41467-024-48592-8.
65. Becker, J.M., et al., *Pathway analysis of Candida albicans survival and virulence determinants in a murine infection model.* Proceedings of the National Academy of Sciences, 2010. **107**(51): p. 22044-22049 DOI: 10.1073/pnas.1009845107.
66. Ianiri, G., et al., *Essential Gene Discovery in the Basidiomycete Cryptococcus neoformans for Antifungal Drug Target Prioritization.* mBio, 2015. **6**(2) DOI: 10.1128/mBio.02334-14.
67. Segal, E.S., et al., *Gene Essentiality Analyzed by In Vivo Transposon Mutagenesis and Machine Learning in a Stable Haploid Isolate of Candida albicans.* MBio, 2018. **9**(5) DOI: 10.1128/mBio.02048-18.
68. Fu, C., et al., *Leveraging machine learning essentiality predictions and chemogenomic interactions to identify antifungal targets.* Nature Communications, 2021. **12**(1) DOI: 10.1038/s41467-021-26850-3.
69. Chung, D., et al., *ChIP-seq and In Vivo Transcriptome Analyses of the Aspergillus fumigatus SREBP SrbA Reveals a New Regulator of the Fungal Hypoxia Response and Virulence.* PLoS Pathogens, 2014. **10**(11) DOI: 10.1371/journal.ppat.1004487.
70. Cheng, S., et al., *Profiling of Candida albicans Gene Expression During Intra-abdominal Candidiasis Identifies Biologic Processes Involved in Pathogenesis.* The Journal of Infectious Diseases, 2013. **208**(9): p. 1529-1537 DOI: 10.1093/infdis/jit335.
71. Xu, W., et al., *Activation and Alliance of Regulatory Pathways in C. albicans during Mammalian Infection.* PLOS Biology, 2015. **13**(2) DOI: 10.1371/journal.pbio.1002076.
72. Amorim-Vaz, S., et al., *RNA Enrichment Method for Quantitative Transcriptional Analysis of Pathogens In Vivo Applied to the Fungus Candida albicans.* mBio, 2015. **6**(5) DOI: 10.1128/mBio.00942-15.
73. Liu, H., et al., *Determining Aspergillus fumigatus transcription factor expression and function during invasion of the mammalian lung.* PLOS Pathogens, 2021. **17**(3) DOI: 10.1371/journal.ppat.1009235.
74. Nielsen, K., et al., *The Aspergillus fumigatus Dihydroxyacid Dehydratase Ilv3A/IlvC Is Required for Full Virulence.* PLoS ONE, 2012. **7**(9) DOI: 10.1371/journal.pone.0043559.
75. Nazi, I., et al., *Role of homoserine transacetylase as a new target for antifungal agents.* Antimicrobial Agents and Chemotherapy, 2007. **51**(5): p. 1731-1736 DOI: 10.1128/Aac.01400-06.
76. Kastanos, E.K., Y.Y. Woldman, and D.R. Appling, *Role of Mitochondrial and Cytoplasmic Serine Hydroxymethyltransferase Isozymes in de Novo Purine Synthesis in Saccharomyces cerevisiae.* Biochemistry, 1997. **36**(48): p. 14956-14964 DOI: 10.1021/bi971610n.
77. Schlüpen, C., et al., *Disruption of the SHM2 gene, encoding one of two serine hydroxymethyltransferase isoenzymes, reduces the flux from glycine to serine in Ashbya gossypii.* Biochemical Journal, 2003. **369**(2): p. 263-273 DOI: 10.1042/bj20021224.
78. Schwertz, G., et al., *Antimalarial Inhibitors Targeting Serine Hydroxymethyltransferase (SHMT) with in Vivo Efficacy and Analysis of their Binding Mode Based on X-ray Cocrystal Structures.*

832 Journal of Medicinal Chemistry, 2017. **60**(12): p. 4840-4860 DOI:
833 10.1021/acs.jmedchem.7b00008.
834 79. Batool, N., et al., *Functional Identification of Serine Hydroxymethyltransferase as a Key Gene*
835 *Involved in Lysostaphin Resistance and Virulence Potential of Staphylococcus aureus Strains.*
836 International Journal of Molecular Sciences, 2020. **21**(23) DOI: 10.3390/ijms21239135.
837 80. Antunes, L.C.M., et al., *Structural and functional insight into serine hydroxymethyltransferase*
838 *from Helicobacter pylori.* Plos One, 2018. **13**(12) DOI: 10.1371/journal.pone.0208850.
839 81. Pu, M., et al., *Serine Hydroxymethyltransferase ShrA (PA2444) Controls Rugose Small-Colony*
840 *Variant Formation in Pseudomonas aeruginosa.* Frontiers in Microbiology, 2018. **9** DOI:
841 10.3389/fmicb.2018.00315.
842 82. Juvvadi, P.R., et al., *Harnessing calcineurin-FK506-FKBP12 crystal structures from invasive*
843 *fungal pathogens to develop antifungal agents.* Nature Communications, 2019. **10**(1) DOI:
844 10.1038/s41467-019-12199-1.
845 83. Gobeil, S.M.C., et al., *Leveraging Fungal and Human Calcineurin-Inhibitor Structures,*
846 *Biophysical Data, and Dynamics To Design Selective and Nonimmunosuppressive FK506*
847 *Analogs.* mBio, 2021. **12**(6) DOI: 10.1128/mBio.03000-21.
848 84. Lee, Y., et al., *In Vitro and In Vivo Assessment of FK506 Analogs as Novel Antifungal Drug*
849 *Candidates.* Antimicrobial Agents and Chemotherapy, 2018. **62**(11) DOI: 10.1128/aac.01627-
850 18.
851 85. Hearn, V.M. and D.W. Mackenzie, *Mycelial antigens from two strains of Aspergillus fumigatus:*
852 *an analysis by two-dimensional immunoelectrophoresis.* Mykosen, 1980. **23**(10): p. 549-62.
853 86. Bertuzzi, M., et al., *On the lineage of Aspergillus fumigatus isolates in common laboratory use.*
854 Medical Mycology, 2021. **59**(1): p. 7-13 DOI: 10.1093/mmy/myaa075.
855 87. Zhao, C., et al., *High-Throughput Gene Replacement in Aspergillus fumigatus.* Current
856 Protocols in Microbiology, 2019. **54**(1) DOI: 10.1002/cpmc.88.
857 88. van Rhijn, N., et al., *Development of a marker-free mutagenesis system using CRISPR-Cas9 in*
858 *the pathogenic mould Aspergillus fumigatus.* Fungal Genetics and Biology, 2020. **145** DOI:
859 10.1016/j.fgb.2020.103479.
860 89. Peng, D. and R. Tarleton, *EuPaGDT: a web tool tailored to design CRISPR guide RNAs for*
861 *eukaryotic pathogens.* Microbial Genomics, 2015. **1**(4) DOI: 10.1099/mgen.0.000033.
862 90. Ralph, B. and D.C. Sheppard, *A Murine Model for Chronic A. fumigatus Airway Infections*, in
863 *Host-Fungal Interactions*. 2021. p. 215-224.
864 91. Amos, B., et al., *VEuPathDB: the eukaryotic pathogen, vector and host bioinformatics resource*
865 *center.* Nucleic Acids Research, 2022. **50**(D1): p. D898-D911 DOI: 10.1093/nar/gkab929.
866 92. Cherinka, B., et al., *Marvin: A Tool Kit for Streamlined Access and Visualization of the SDSS-IV*
867 *MaNGA Data Set.* The Astronomical Journal, 2019. **158**(2) DOI: 10.3847/1538-3881/ab2634.
868 93. Haberthür, U. and A. Caflisch, *FACTS: Fast analytical continuum treatment of solvation.* Journal
869 of Computational Chemistry, 2007. **29**(5): p. 701-715 DOI: 10.1002/jcc.20832.

870

871

872 **FIGURE CAPTIONS**

873 **Figure 1. Identification of genes potentially relevant *for Aspergillus fumigatus* virulence using**
874 **NanoString *in vivo* transcriptomics.**

875 **A)** Validation of the linear amplification performed with the Nanostring Single Cell Gene Expression
876 protocol with Multiplexed Target Enrichment (MTE) primers. The fold changes between diluted-
877 amplified and non-amplified (undiluted) *in vitro* (-S limiting conditions) and *in vivo* samples (lungs
878 extracted from two leukopenic mice 72h after infection) were compared. For both mice, there was a
879 linear relationship between the FCs of non-amplified and amplified samples, demonstrating that
880 amplification did not affect the relative abundance of transcripts. **B)** Hierarchical clustering of all
881 samples formed two distinct branches, one of *in vitro* samples and one with the *in vivo* samples. There
882 were 15 genes (red line) that were always expressed at higher levels in the *in vivo* samples, compared
883 with all the *in vitro* samples.

884 **Figure 2. The fungal S-related sulfur metabolism *in vivo* is influenced by the model of suppression**
885 **and the time of infection.**

886 **A)** Hierarchical clustering of all *in vivo* samples created two major branches, one almost exclusive for
887 leukopenic samples, which only included the chronic model sample. The second major branch was
888 divided again in two branches, one exclusive for steroid samples and the other mixed with leukopenic
889 and steroid samples. Therefore, the model of suppression influences but is not the only factor that
890 determines the fungal metabolic status. **B)** Separated hierarchical clustering of leukopenic or steroid
891 samples partially aggregated by the time of infection. Therefore, the fungal S-related metabolism is
892 influenced *in vivo* by the status of infection.

893 **Figure 3. Temporal dynamics of gene expression reveals the existence of potential initiation and**
894 **disease progression factors.**

895 **A)** Fold change of expression of genes in each time-point with respect to the correspondent 16h
896 condition revealed that most genes changed expression during the course of infection. The geometric
897 mean value for each time-point was used. **B-F** panels display the Log2 fold change (FC) of genes that
898 showed temporal dynamic expression in five randomly selected representative *in vitro* condition (in
899 order: -N, -S, 0.1 mM Cys, 2 mM SH_2 and 5 mM Met) versus *in vivo* conditions. All graphs display the
900 mean and the standard error of the mean (SEM). **B)** These five genes always showed higher expression
901 at early (16h) than at mid- or late (24h or 72h) infection of leukopenic mice when compared with the
902 *in vitro* conditions. **C)** In leukopenic mice, the gene *cdoA* consistently showed the highest level of
903 expression at late infection, when compared with the *in vitro* conditions. **D)** These three genes always

904 showed higher expression at early and late (16 and 72h) than at mid- (24h) infection of leukopenic
905 mice, when compared with the in vitro conditions. **E)** The four genes consistently showed higher
906 expression at mid- and late infection than at early infection, when compared with the *in vitro*
907 conditions. **F)** These 9 genes always showed the highest level of expression at mid- (24h) than at early
908 or late infection, when compared with the *in vitro* conditions.

909 **Figure 4. The cytosolic serine hydroxymethyltransferase is essential for viability and virulence in**
910 ***Aspergillus fumigatus***.

911 **A)** A ShmB-Citrine tagged proteins localised diffused throughout the cytoplasm, similarly as the control
912 P*gdpA*-Citrine strain.**B)** A Phenotypic assay with two independent clones of the *shmB_tetOFF* and
913 *ΔshmA shmB_tetOFF* mutant strains. In the presence of doxycycline (Dox) the mutants did not grow,
914 demonstrating that *shmB* is essential in *A. fumigatus*, and that ShmA cannot cover its function. Plates
915 were incubated for 48h at 37 °C. The experiment was repeated twice independently. **C)** Attempting to
916 reconstitute *shmB_tetOFF* growth in restrictive conditions (+Dox), media was supplemented with
917 various metabolites which could potentially be limited in the absence of serine
918 hydroxymethyltransferase activity. The only condition that could partly reconstitute growth, not at
919 wild-type level, was supplementation with ATP and adenine (Ade). Plates were incubated for 48 h at
920 37 °C. The experiment was repeated twice independently. **D)** Dox (10 µg/mL) was added or not to 12h
921 grown submerged mycelia of the *shmB_tetOFF* and its parental strains. Measurements of fungal
922 biomass at 20h, 36h and 40h post-inoculation showed a significant reduction of growth after
923 downregulation of *shmB.* The experiment was repeated three times independently, with three
924 technical replicates. The results were analysed using a one-way ANOVA with Tukey's multiple
925 comparisons test. * = $p<0.05$ and ***=$p<0.001$ **E)** Fungal burden in the lungs of leukopenic mice
926 treated or untreated with Dox. Downregulation of *cyp51A* (encoding the target of the azoles)
927 expression caused a significant reduction in burden ($p=0.0159$ in a nonparametric Mann Whitney test
928 and $p=0.0476$ in an unpaired *t*-test with Welch's correction). Similarly, downregulation of *shmB*
929 triggered a significant decrease in fungal burden ($p=0.0159$ in a nonparametric Mann Whitney test
930 and $p=0.0288$ in an unpaired *t*-test with Welch's correction). Therefore, ShmB appears to be a valid
931 antifungal target. Each point represents an independent mouse (biological replicate) and the graph
932 shows the mean and the standard of the mean (SEM). Comparisons were made using a Mann-Whitney
933 non-parametric *t*-test.

934 **Figure 5. An inhibitor of the human SHMT does not bind properly to the fungal enzyme's ligand**
935 **binding pocket**

936 **A)** Binding pockets with draggability score above 0.5 predicated by DrupRep highlighted in human
937 SHMT1 1bj4, with 'Pocket A' Zoomed in (left corner). **B)** Alignment of the amino acid sequences
938 (partial) of the *A. fumigatus* (ShmB) and human (SHMT1) cytosolic SHMT enzymes. Different amino
939 acids (highlighted in red rectangles) were detected surrounding the key residues Arg263 in SHMT1
940 (Arg255 in ShmB, highlighted in blue rectangle); and Arg43 (Arg35 in ShmB, highlighted in green
941 rectangle). Orange arrows indicate SHMT1 residues forming hydrogen bonds with Hit-1 and purple
942 arrow indicates ShmB residue forming hydrogen bond with Hit-1. **C)** Predicted binding pockets
943 comparison between SHMT1 and ShmB with Arg263 (Arg255) highlighted in red. **D)** Hit-1 binding
944 motifs suggested by SwissDock. **E)** Detailed interactions formed between Hit-1 and SHMT1. **F)** Detailed
945 interactions formed between Hit-1 and ShmB. **G)** List of hydrogen bond pairs between Hit-1 and
946 SHMT1 and ShmB.

947 **SUPPLEMENTARY FIGURES**

948 **Fig. S1. Quality Control of NanoString run**

949 **A)** Total number of positive counts (included in the codeset) detected in each condition. **B)** Total
950 number of counts (excluding positive and negative controls) in each condition. All conditions reached
951 the required thresholds except the samples Leukopenic 1.2 and leukopenic 1.3, which were eliminated
952 from all analyses.

953 **Fig. S2. Temporal dynamics of gene expression**

954 Fold change of all genes in each *in vitro* condition versus each of the **A)** leukopenic samples and **B)**
955 corticosteroid ordered by the time after infection identified temporal dynamics in the expression of
956 certain genes.

957 **Fig. S3. Shm supplementary data**

958 **A)** Alignment of the amino acid sequences of the two serine hydroxymethyltransferase enzymes
959 encoded in *A. fumigatus* genome. The proteins have 61.9% identity and 79.9% similarity. ShmA has a
960 long N-terminus region that is absent in ShmB and which after further analysis (see text) suggests that
961 ShmA is mitochondrial. **B)** Alignment of the amino acid sequences of *A. fumigatus* (ShmA and ShmB)
962 and *S. cerevisiae* (SHM1 and SHM2) serine hydroxymethyltransferase proteins. As the yeast
963 mitochondrial enzyme SHM1, ShmA shows an elongated N-terminus, suggesting that this is the
964 mitochondrial enzyme in *A. fumigatus*. **C)** Two independent transformants of *ΔshmA* grew normally
965 on both Sabouraud (SAB) rich and minimal (MM) media, proving that this gene is not essential. **D)**
966 Transcription of *shmB* in the *shmB_tetOFF* strain decreased very strongly upon Dox addition. Graph
967 depicts the mean and the SD. Data was analysed with one-way ANOVA with Dunnett's multiple
968 comparisons, $p < 0.001$.

969 **Fig. S4. Colistin permeabilises the membrane of *A. fumigatus* swollen conidia**

970 Swollen conidia are impermeable to the dyes FITC and Zombie-Aqua™. However, when germinated in
971 the presence of 4 µg/mL colistin these dyes were able to penetrate inside the cells, demonstrating
972 that the membrane has been permeabilised. A) Image of the central plane of a z-stack covering the
973 full field of view. B) Zoom of individual conidia at their own central plane.

974 **Fig. S5. Hierarchical clustering with two additional mice**

975 The inclusion of two extra mice (from the experiment described in Figure 1A) did not substantially
976 modified the expression profile, although the two mice clustered separated from the rest (purple
977 arrow). There was still a complete separation of *in vitro* and *in vivo* samples, and the same 15 genes

978 identified before as always expressed at higher levels (red line) were maintained. Additionally, one
979 more gene got included in this list, AFUA_5G07210 (red arrow), encoding a homoserine O-
980 acetyltransferase.

981

982 **SUPPLEMENTARY FILES**

983 **Table S1**: Genes included in the NanoString custom codeset.

984 **Table S2**: *In vitro* and *in vivo* conditions assayed for the NanoString run.

985 **Table S3**: Primers employed in this study.

986 **Supplementary File 1**: NanoString designed Probes A and B for hybridisation and MTE primers for
987 enrichment.

988 **Supplementary File 2**: Raw data from digital analysis of hybridised codesets.

989 **Supplementary File 3:** Normalized data used for the analyses.

Fig. 1

A

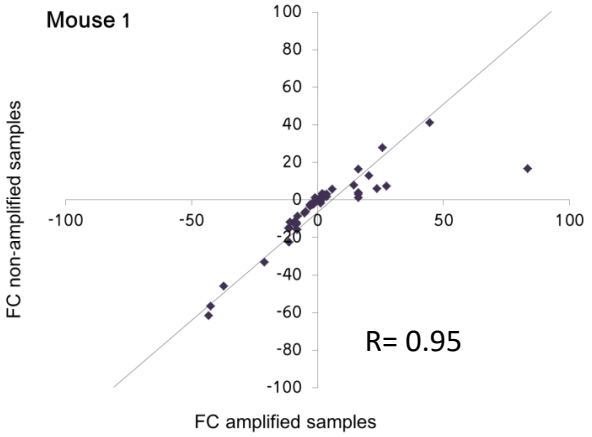
Mouse 1
FC non-amplified samples
FC amplified samples
R= 0.95

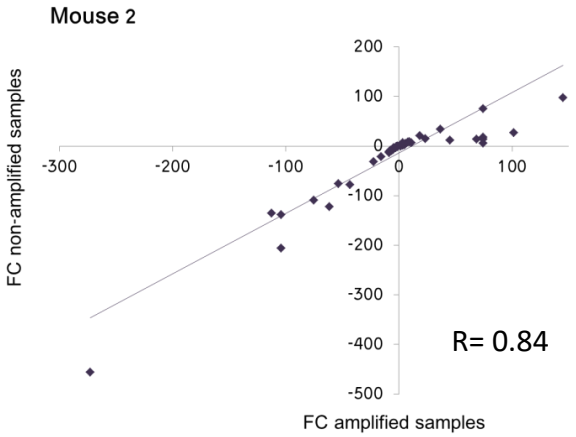
Mouse 2
FC non-amplified samples
FC amplified samples
R= 0.84

B

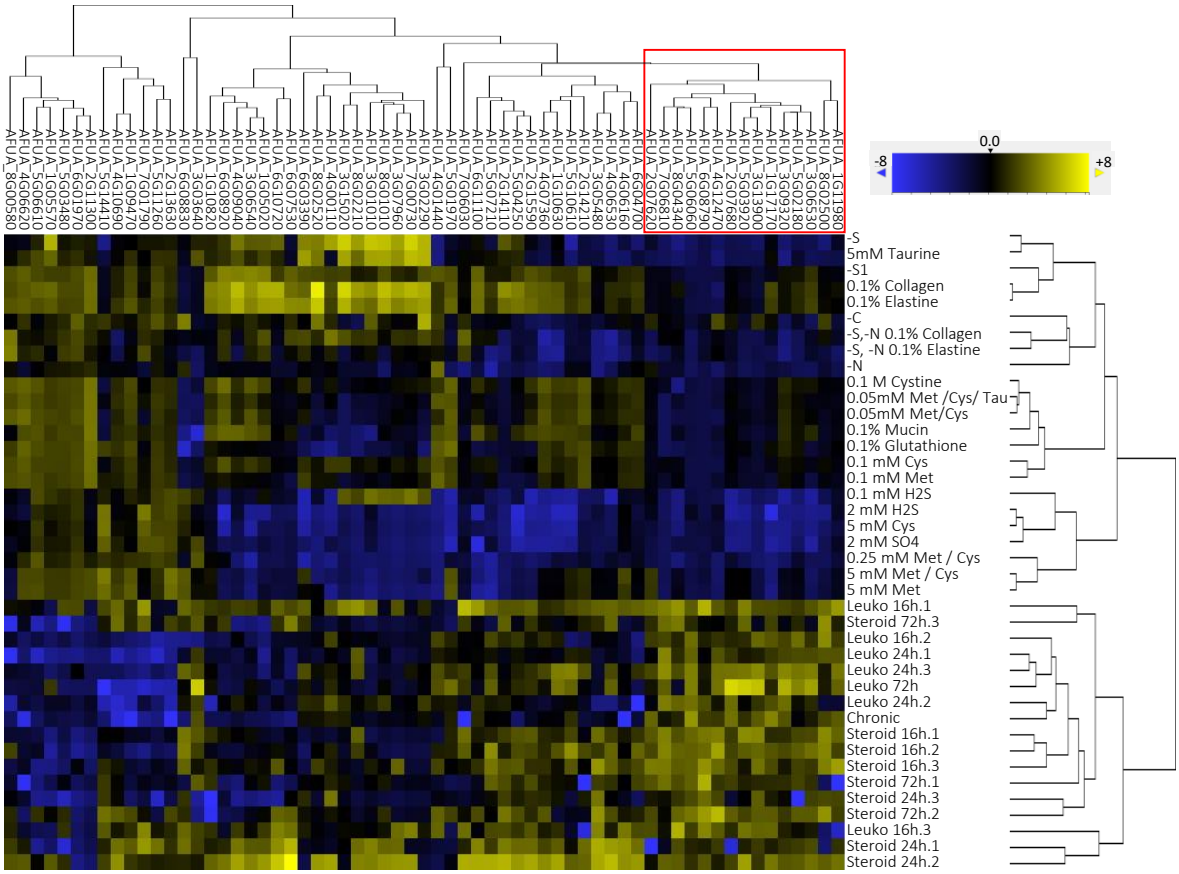
-S
5mM Taurine
-S1
0.1% Collagen
0.1% Elastine
-C
-S,-N 0.1% Collagen
-S, -N 0.1% Elastine
-N
0.1 M Cystine
0.05mM Met /Cys/ Tau
0.05mM Met/Cys
0.1% Mucin
0.1% Glutathione
0.1 mM Cys
0.1 mM Met
0.1 mM H2S
2 mM H2S
5 mM Cys
2 mM SO4
0.25 mM Met / Cys
5 mM Met / Cys
5 mM Met
Leuko 16h.1
Steroid 72h.3
Leuko 16h.2
Leuko 24h.1
Leuko 24h.3
Leuko 72h
Leuko 24h.2
Chronic
Steroid 16h.1
Steroid 16h.2
Steroid 16h.3
Steroid 72h.1
Steroid 24h.3
Steroid 72h.2
Leuko 16h.3
Steroid 24h.1
Steroid 24h.2

Fig. 2

A

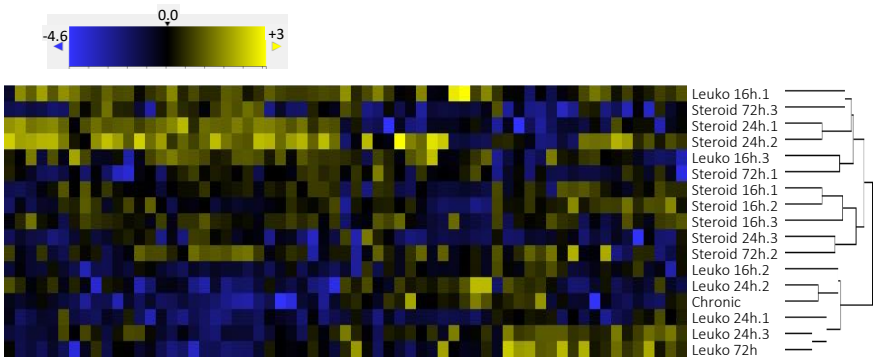
0.0
-4.6
+3
Leuko 16h.1
Steroid 72h.3
Steroid 24h.1
Steroid 24h.2
Leuko 16h.3
Steroid 72h.1
Steroid 16h.1
Steroid 16h.2
Steroid 16h.3
Steroid 24h.3
Steroid 72h.2
Leuko 16h.2
Leuko 24h.2
Chronic
Leuko 24h.1
Leuko 24h.3
Leuko 72h

B

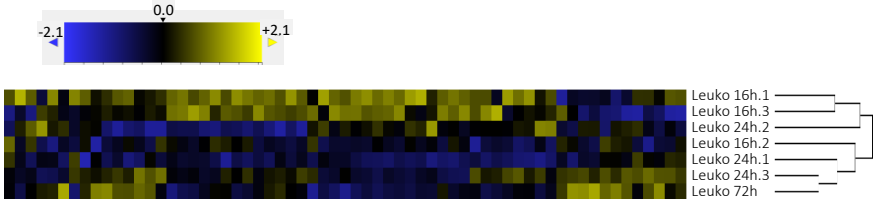
0.0
-2.1
+2.1
Leuko 16h.1
Leuko 16h.3
Leuko 24h.2
Leuko 16h.2
Leuko 24h.1
Leuko 24h.3
Leuko 72h

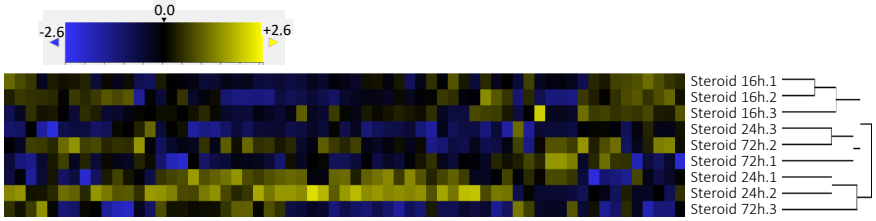
0.0
-2.6
+2.6
Steroid 16h.1
Steroid 16h.2
Steroid 16h.3
Steroid 24h.3
Steroid 72h.2
Steroid 72h.1
Steroid 24h.1
Steroid 24h.2
Steroid 72h.3

Fig. 3

A

Leuko 16h
Leuko 24h
Leuko 72h
VS Leuko 16h
0.0
-8
+8
Steroid 16h
Steroid 24h
Steroid 72h
VS Steroid 16h

B

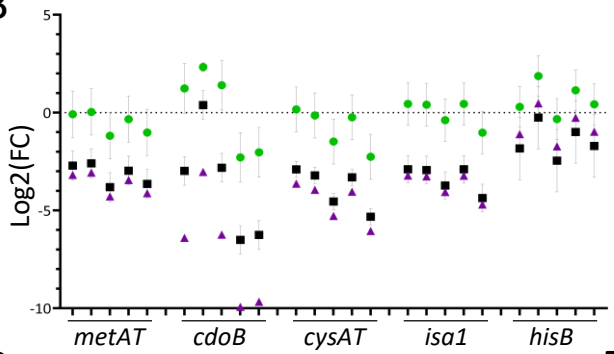
Log2(FC)
metAT
cdoB
cysAT
isa1
hisB

C

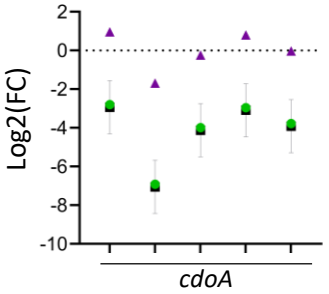
Log2(FC)
cdoA

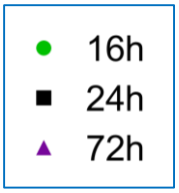
16h
24h
72h

D

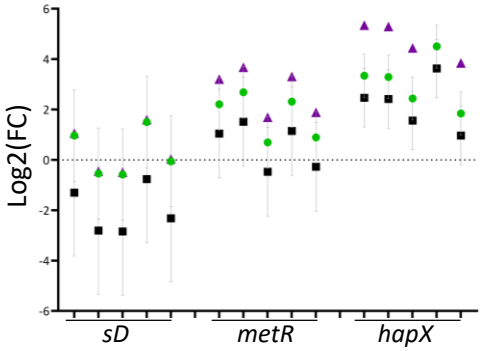
Log2(FC)
sD
metR
hapX

E

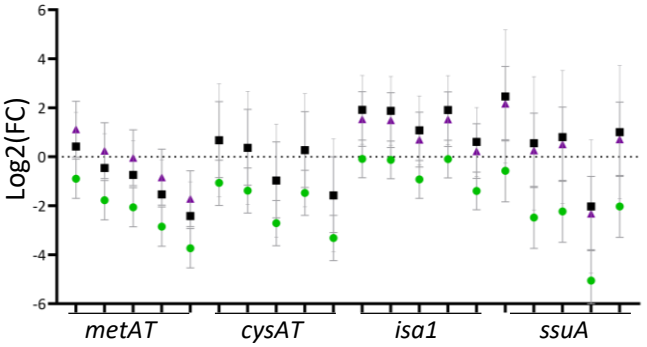
Log2(FC)
metAT
cysAT
isa1
ssuA

F

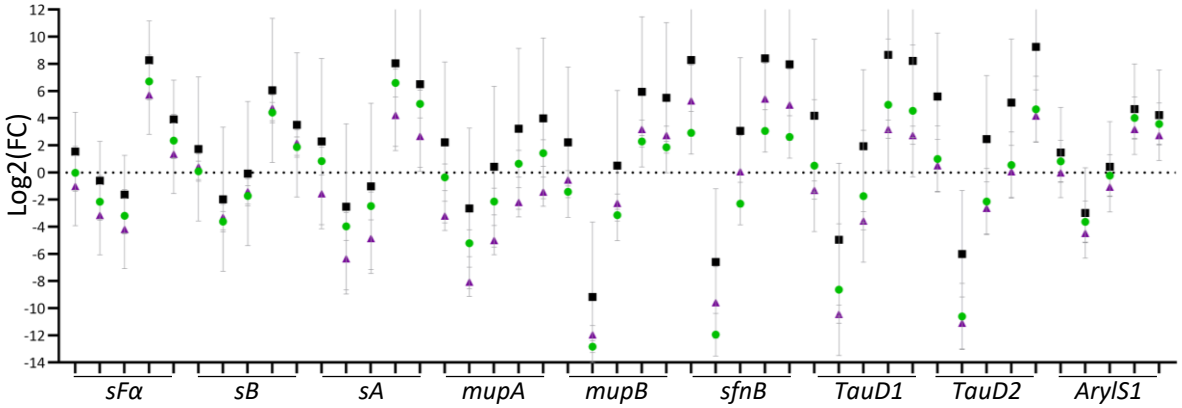
Log2(FC)
sFα
sB
sA
mupA
mupB
sfnB
TauD1
TauD2
ArylS1

Fig. 4

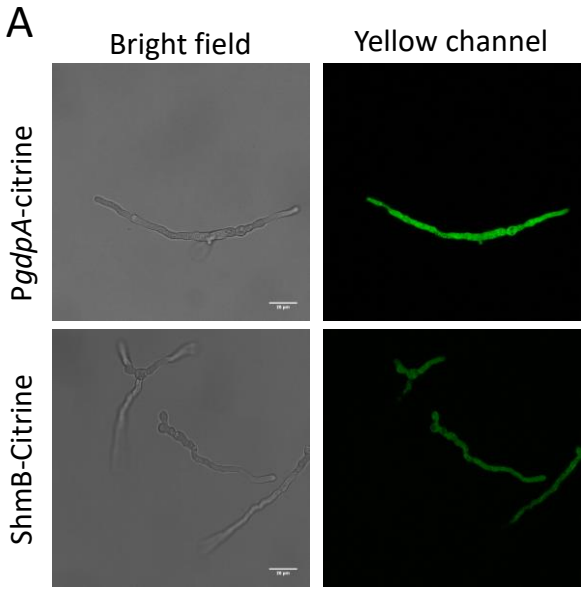
A
Bright field
Yellow channel
PgdpA-citrine
ShmB-Citrine

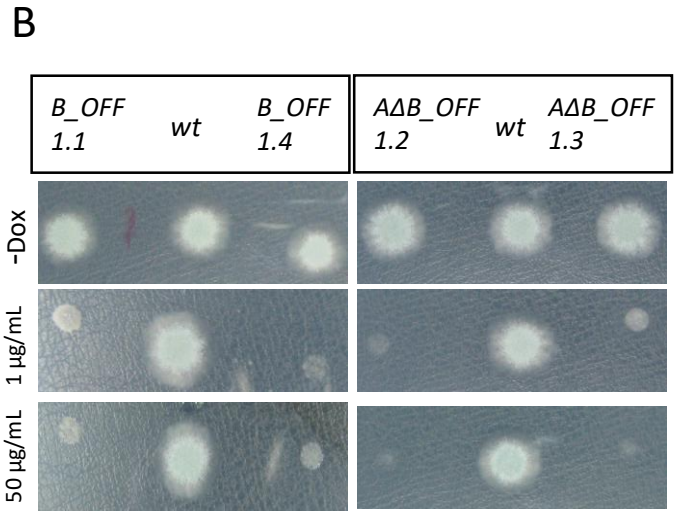
B
B_OFF 1.1
wt
B_OFF 1.4
AΔB_OFF 1.2
wt
AΔB_OFF 1.3
-Dox
1 µg/mL
50 µg/mL

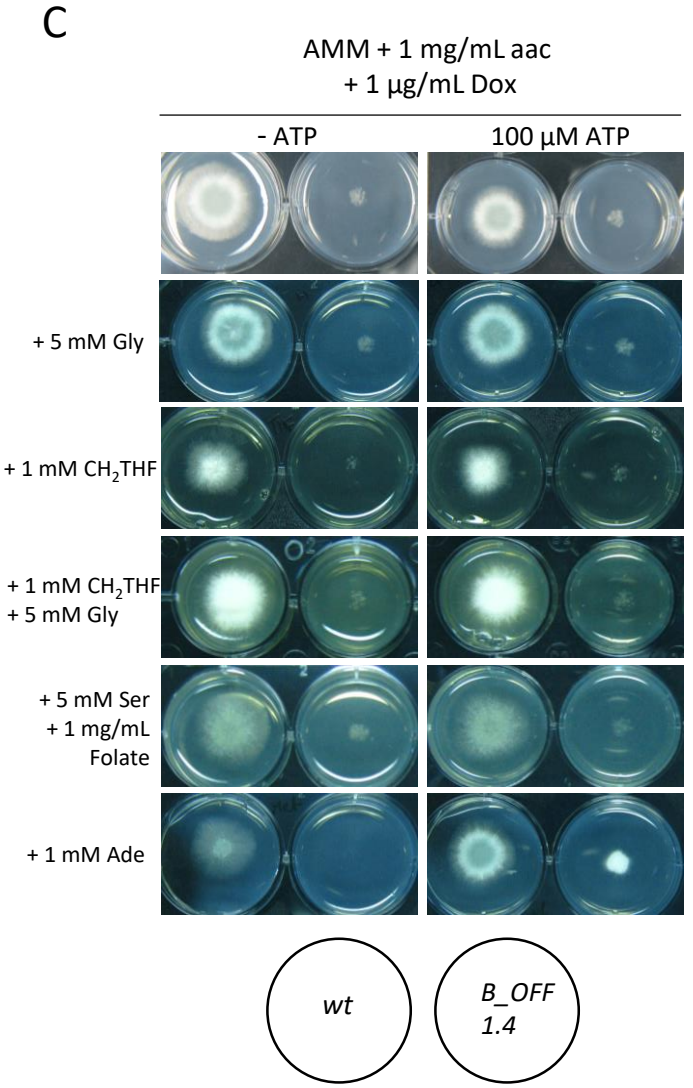
C
AMM + 1 mg/mL aac
+ 1 µg/mL Dox
- ATP
100 µM ATP
+ 5 mM Gly
+ 1 mM CH2THF
+ 1 mM CH2THF
+ 5 mM Gly
+ 5 mM Ser
+ 1 mg/mL
Folate
+ 1 mM Ade
wt
B_OFF
1.4

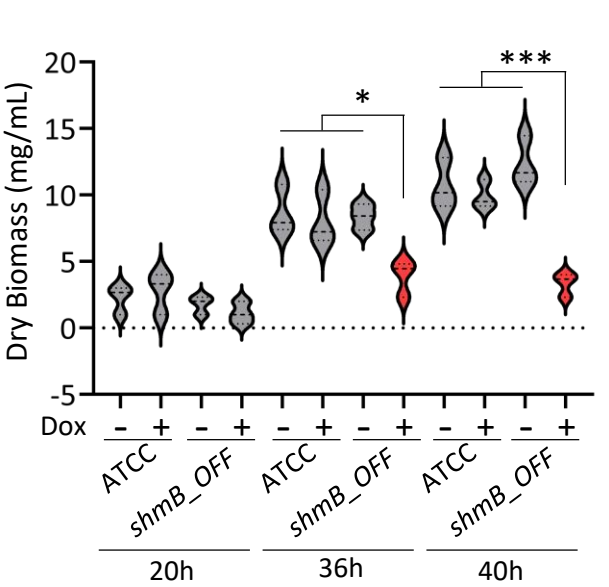
D
Dry Biomass (mg/mL)
20
15
10
5
0
-5
*
***
Dox
-
+
ATCC
shmB_OFF
20h
36h
40h

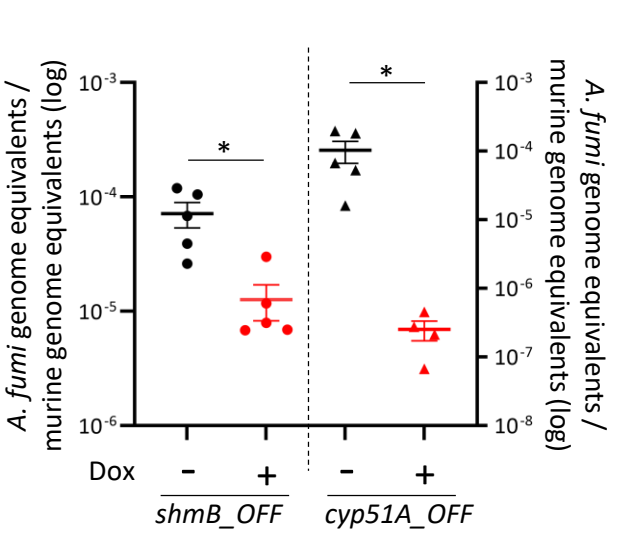
E
A. fumi genome equivalents / murine genome equivalents (log)
10-3
10-4
10-5
10-6
10-7
10-8
*
Dox
-
+
shmB_OFF
cyp51A_OFF

Fig. 5

A

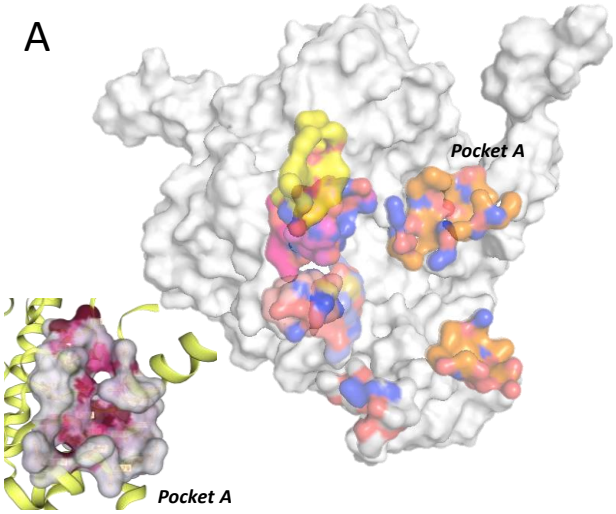

Pockets	Vol. Hull	Hydroph. Kyte	Polar Res	Aromtica Res	Drugg Prob	Standard Deviation
P1	667.66	0.18	0.47	0.20	**0.89**	**0.03**
P2	557.96	-0.03	0.50	0.06	**0.68**	**0.04**
P6	429.67	-0.03	0.42	0.08	**0.70**	**0.03**
P7	439.19	0.10	0.33	0.11	**0.79**	**0.01**
P8	407.80	-0.44	0.50	0.21	**0.69**	**0.06**
P9	473.76	0.22	0.40	0.00	**0.73**	**0.07**

B

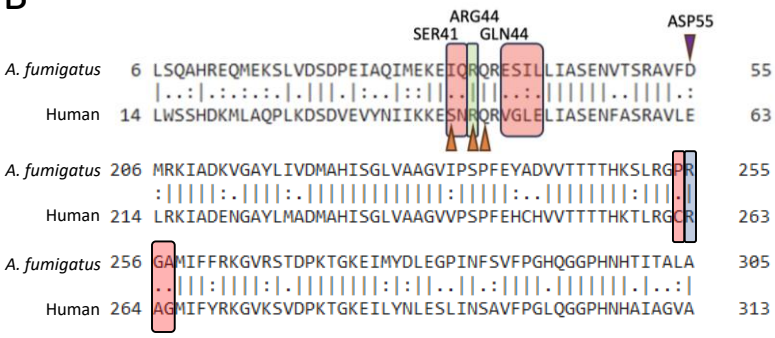

C

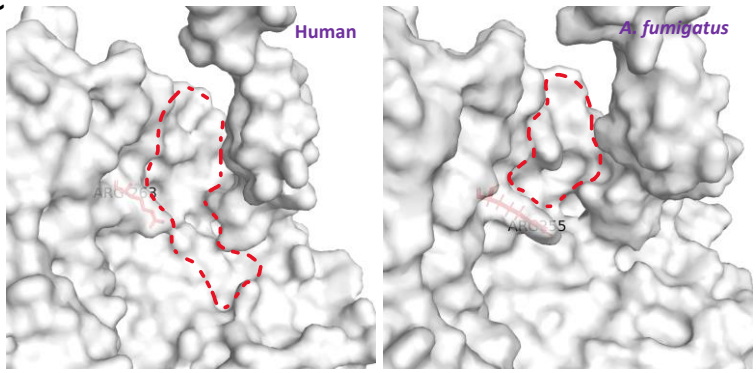

D

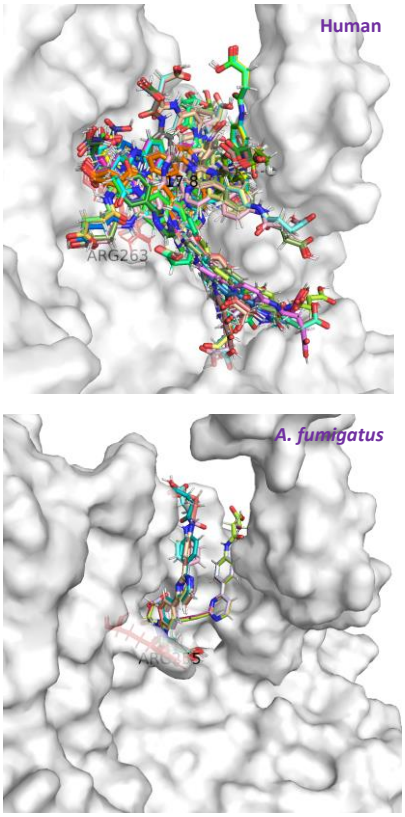

E

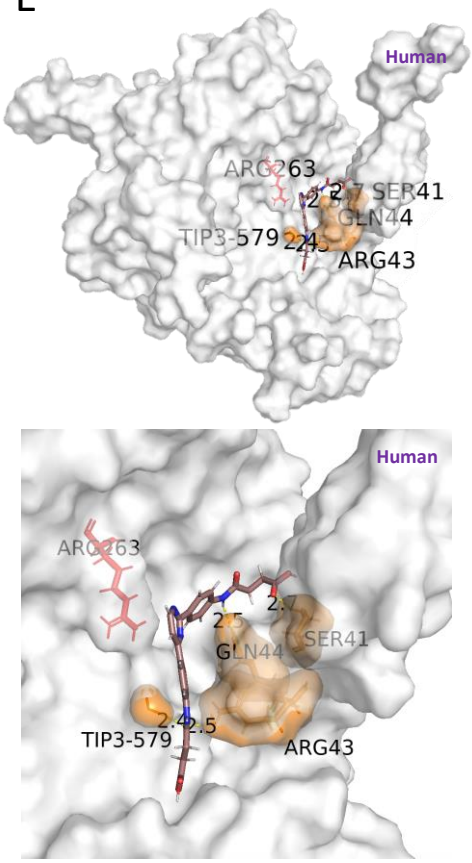

F

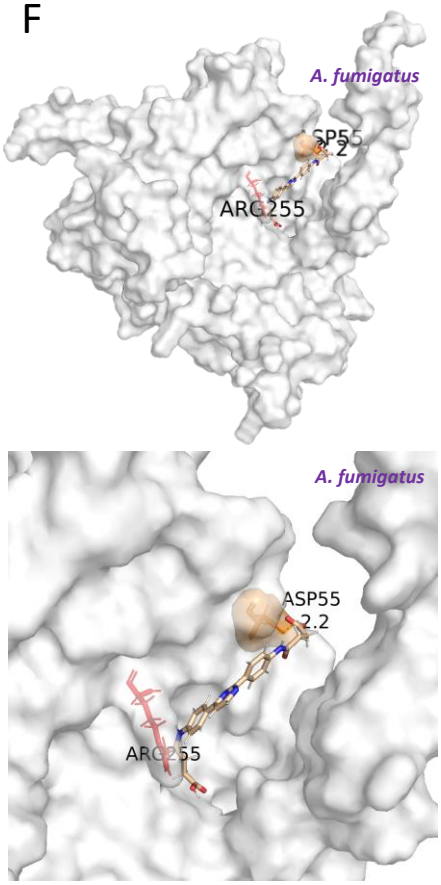

G

Hydrogen bond pairs between Hit-1 and SHMT					
Distance	2.7	2.5	2.5	2.4	2.2
Hit-1	HIT1.242/O5	HIT1.242/H16	HIT1.242/O2	HIT1.242/O2	HIT1.28/ H21
Human	SER`41/HG1	GLN`44/OE1	ARG`43/HH21	TIP3`579/H1	
A. fumigatus					ASP`55/OD1

The unit of the distance measuring is Å.